Application and calibration of 2-dimensional flowmodel for small tidal rivers with insufficienthydrographic data in Vietnamese Mekong Delta （限定的な水路情報に基づくメコンデルタ小感潮河川への2次元流れモデルの適用と較正）

Doctoral Dissertation

APPLICATION AND CALIBRATION OF 2-DIMENSIONAL FLOW MODEL FOR SMALL TIDAL RIVERS WITH INSUFFICIENT HYDROGRAPHIC DATA IN VIETNAMESE MEKONG DELTA

September 2020

Graduate School of Marine Science and Technology
Tokyo University of Marine Science and Technology
Doctoral Course of Applied Marine Environmental Studies

NGUYEN VAN KHANH

Abstract

In recent years, in the Vietnamese Mekong Delta (VMD) riverbank erosion and collapse have been excessively occurring in many rivers, especially in small rivers, and threatening people living near the riverbank not only their properties but also their future, even their lives. Erosion and collapse are predicted to increase significantly under the influence of tidal range, sea-level rise (SLR), and land subsidence. To confront with erosion and riverbank collapse, small rivers should be intensively studied together with large rivers as most recent studies. However, making research on small rivers in VMD, especially in modeling a depth-averaged two-dimensional (2-D) flow model, will be very difficult because of the lack of hydraulic data. The main objective of this study is to demonstrate how to apply and calibrate a 2-D flow model for small tidal rivers in the VMD with insufficient hydrodynamic data.

Three primary problems on applying a 2-D flow model to these kinds of small tidal rivers are insufficient bathymetric data, insufficient data for setting up the open boundary conditions, and insufficient data for calibrating the parameters of the model. To solve these problems the following steps were proposed. First, two measurement campaigns were conducted to collect the field data, including depth samples along the river in zigzag distribution, total discharge at the upstream cross-section in 36 hours, daytime hourly water levels near the estuary of the study river (i.e. My Thanh River, Soc Trang Province, Vietnam). Next, a new searching method was proposed as an effective interpolation method to reproduce the river bathymetry with sparse zigzag depth data. Based on the estimated bathymetry, the method suggested by Takagi *et al.* (2019) was applied to a 2-D flow model for the study river with some modifications. Finally, the spatio-temporal velocity along the river recorded by Acoustic Doppler Current Profiler (ADCP) devices during the measurement campaigns was applied to re-calibrate and optimize the 2-D flow model.

Four primary results were obtained at this research. First, a proposed searching method, named Curvilinear search, is the most suitable to apply with Inverse distance weighting (IDW), Ordinary Kriging (OK), and Radial Basis Functions (RBF) interpolation methods to estimate the bathymetry of the river using sparse zigzag data; and two regional interpolation methods (i.e. Curvilinear-IDW method for estimating the near riverbank areas combining with Curvilinear-RBF or Rectilinear-RBF method for estimating the middle river area, respectively) working effectively with this kind of data were also figured out. Second, it was

found that the Riemann boundary condition is very helpful in case of insufficient upstream discharge data but needs to be modified to be compatible with the 2-D flow model. Third, the suggested flow model was improved significantly after re-calibrating with spatio-temporal velocity, reviewing the primary tidal constituents, considering the upstream discharge, and downstream tributary. Particularly, Root-Mean-Square Error (RMSE) of estimated water levels near downstream, upstream, and depth-averaged velocity over upstream cross-section were declined by 50%, 9%, and 12%, respectively; the estimated spatio-temporal velocity was also optimized 16%. Finally, it was demonstrated that the proposed 2-D flow model can be easily applied to simulate the flow of a small tidal river in a long period by applying downstream tidal data and Riemann Boundary. This research will be helpful for other studies with similar field conditions in the future.

Table of contents

List of figures

List of tables

Chapter 1 Introduction

1.1 Problem review and motivation

Recently, erosion and riverbank collapse are important issues in the VMD which are happening in many rivers, especially in small rivers. Based on local news (Tuoitrenews, 2018), by June 2018, there are totally 562 locations where coastal and riverbank subsidence and collapse occurred in the VMD with 55 especially dangerous locations. To take the action, the Vietnamese government decided to provide about 66 million USD to help people living in influenced areas and prevent riverbank collapse in the future.

Three possible reasons for erosion and riverbank collapse have been pointed out by many studies. The first reason is that suspended sediment has trapped by upstream anthropogenic activities such as dams, reservoirs, reforestation, and soil-conservation (Thi Ha *et al.*, 2018; Kondolf *et al.*, 2018). The second reason is sand or river bed mining activities serving for various purposes (Kondolf *et al.*, 2018). The last reason is boat-induced waves (Trung, 2018). However, it is said that most of the recent studies have only been conducted in large river systems in the VMD such as Tien River and Hau River (Bassac River) (Figure 1-1). Small rivers should be investigated right now to find out the reasons and suitable countermeasures should be proposed to reduce the erosion and bank collapse in this river system.

Besides, erosion and collapse are also predicted to increase significantly under the influence of tidal range, SLR, and land subsidence. The erosion will be increased under the interactive effect between SLR and global warming via increasing soil erosion in the catchment basins and sediment flows to the ocean causing by very grim flood ((Zhang *et al.*, 2013). Located in the low-land region, the VMD is very vulnerable to the effect of SLR, especially in the case of the VMD has been facing land subsidence by groundwater pumping (Takagi *et al.*, 2019). As a result, the erosion will increase if the local government does not take any action immediately. So, simulating the erosion in small tidal rivers with SLR projection is also very important in the VMD.

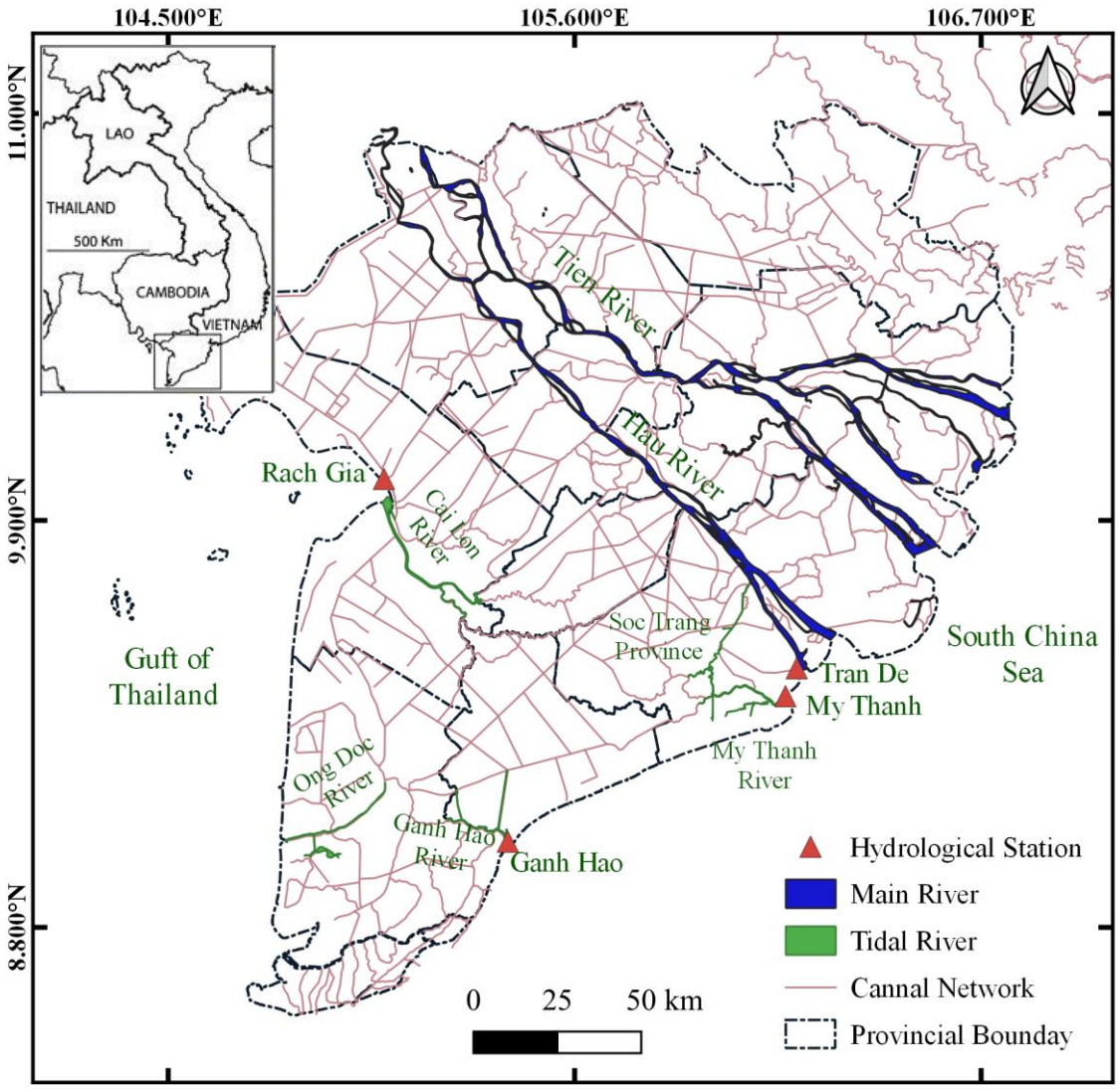

Figure 1-1. The Vietnamese Mekong Delta.

However, in Vietnam, water level gauges are only available in the coastal regions and main rivers. Most of the small rivers are lack of hydraulic data or only have water level data. This is a reason why many studies have been commonly conducted in large rivers. It is considered that the causes and mechanisms of erosion and riverbank collapse can be different between large and small rivers. To find out the reasons for them in the small tidal rivers, the first important step is to simulate the flow field with insufficient hydrodynamic data which are the cases in the small rivers in the VMD. Based on the flow model, other studies such as sediment transport, bed composition, bed morphology

development, riverbank erosion or failure, SLR projection, and so on can be easily performed. However, applying the 2-D/3-D flow model of the tidal rivers with insufficient data is the difficult works as mentioned in the following.

An extensive field measurement must be conducted to collect hydrodynamic data, especially topographic data to estimate river bathymetry. The modern equipment as LiDAR or remote sensing may be difficult to deploy on the rivers in the VMD to obtain the high-resolution dataset because the rivers in this area are very deep and high turbidity. Measuring cross-sectional data is also an ineffective measurement strategy because of high water velocity, heavy traffic load, difficult to access the natural banks of the rivers in this area.

Measuring the data for configuring open boundary conditions of the 2-D flow model is also other problems, especially for the upstream open boundaries. Commonly, upstream open boundaries are described by water discharge. The discharge of tidal rivers must be measured continuously because of its direction changes due to the stages of the tide. Hence, the quality of measured discharge data is not guaranteed because the measurements are under the influence of many factors like weather, water turbidity, or human ability. A method can configure the upstream boundaries with the least measured data is very helpful for deploying the 2-D flow model on small tidal rivers in the VMD or other regions with similar conditions.

Calibrating the parameters of the 2-D flow model of tidal rivers in the VMD is also an issue. Tidal rivers in this area are under the multiple effects of tide, upstream freshwater discharge, tributary channels, so calibrating the parameters of their flow model based on measured data at some specific locations as recent studies is not an effective method because these data might not well represent the real river flow. The spatio-temporal data as velocity measured by the ADCP device during depth measurement periods should be applied for calibrating the flow field of the flow model to consider the above effects to the calibrating process.

This aim of this research is to apply and calibrate the 2-D flow model for a small tidal river with insufficient hydrographic data in the VMD based on solving these above difficulties step by step.

1.2 Research objectives

The overall objective of the research is to demonstrate the application and calibration of the 2-D flow model for small tidal rivers with inadequate hydrographic data in the VMD to support for studying other fluvial processes in the future.

The specific objectives are:

- To propose a new searching method as an effective interpolation method to estimate the river bathymetry with sparse depth data;

- To model the 2-D flow model of small tidal rivers with insufficient hydrodynamic data;

- To improve the proposed 2-D flow model by reviewing the tidal data and re-calibrating its parameters by using the spatio-temporal velocity records measured by the ADCP device.

1.3 Study area and data

This study was conducted in My Thanh River, the main tidal river of Soc Trang province that lies off the East coast of Southern Vietnam (Figure 1-1 and Figure 1-2). This river drains directly to the East Sea (South China Sea), and the upstream bifurcates into two main channels and a complex canal network toward the in-land area. Its upstream also connects to the Hau River (Bassac River), so its flow regime is under the multi-influence of the semidiurnal tidal regime of the East Sea, Hau River, and upstream channels. Many people are living near the riverbank by doing agriculture and aquaculture. This river was selected because it can represent other small tidal rivers in VMD.

Only tidal data at My Thanh station are available but only from 1985 to 2007. After this period, this station was already stopped but tidal data at Tran De station at Bassac estuary, about 10 km from the old station (Figure 1-1) can be used. However, in this study, the tidal data at Tran De station could be found only from 2008 to 2014.

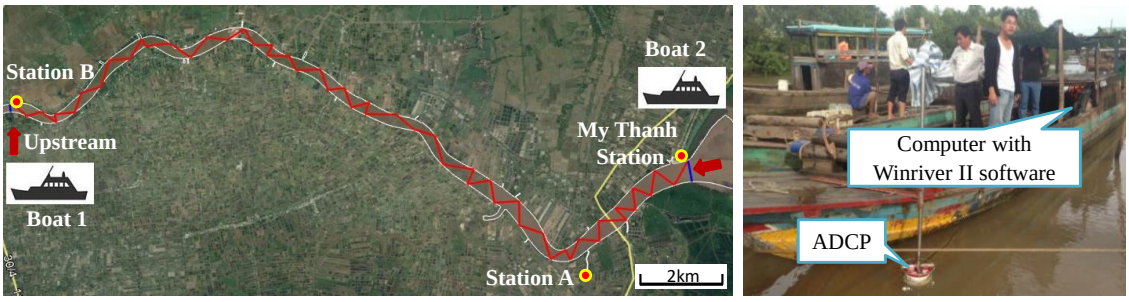

(a) (b)

Figure 1-2. My Thanh River with field observation overall planning (a), and equipment setup (b).

Besides, two same field measurement campaigns were conducted in My Thanh River on 16th, 17th June, and 28th, 29th August 2018 to collect necessary field data. The measurement length is approximately 22km from the estuary. Figure 1-2 (a) depicts the layout of these measurements to collect hydraulic data of My Thanh River such as discrete depth samples, discharge and velocity, and water level. In each campaign, two teams were needed to run these measurements. The first team operated the Boat 1 across the river at the upstream location every hour to get water velocity and discharge by using an ADCP device installed on the boat as in Figure 1-2 (b). Simultaneously, the other team operated the Boat 2 along the river to collect the discrete depth samples also by an ADCP. Boat 2 followed a zigzag trajectory as shown by the red line in Figure 1-2 (a). Additionally, half-hourly water level data were also recorded manually at two observation locations Station A and Station B by using rulers. The measured data in June and August 2018 were used for validation and calibration of the 2-D flow model of My Thanh River, respectively.

1.4 Thesis outline

This thesis is comprised of six chapters that include the introduction (Chapter 1) and conclusions (Chapter 6). The body chapters (Chapters 2 to 5) follow the research objectives indicated above.

Chapter 2 shows the overall review of the related studies, including hydrodynamic models and its applications, modeling the flow of small tidal rivers using Riemann Boundary, and river topography interpolations.

Chapter 3 presents a new searching method for finding samples to estimate the bathymetry of rivers which can be combined with common interpolators to estimating three-dimensional (3-D) river shape from sparse zigzag depth data. It has been shown to be excellent in shape estimation near the riverbank, especially in curved areas.

Chapter 4 describes a 2-D flow model of the study river which is applied the Riemann boundary condition proposed by Takagi *et al.* (2019) is improved by considering the flow velocity loss near the riverbank, and the boundary condition at the upstream end is given.

Chapter 5 concentrates on improving the 2-D flow model in Chapter 4 by reviewing the tidal level measured at the river mouth and nearby station, and the model was calibrated and optimized using the spatio-temporal velocity records measured by ADCP device to significantly improve the reproducibility of the flow field.

Chapter 2 Literature review

2.1 Hydrodynamic model

Hydrodynamic models are applied to illustrate the flow field as direction and magnitude, and depths of the river for various conditions of flow. Hydrodynamic modeling can be classified into three main groups based on the used equations and the computational domain, including: one-dimensional (1-D), two-dimensional (2-D), and three-dimensional (2-D).

2.1.1 1-D Hydrodynamic model

1-D model is the simplest option that describes the flow conditions within a river by a set of cross-sections. The simplest form of the 1-D model solves one-dimensional energy equations to compute water-surface elevations at each cross-section for steady gradually varied flow conditions. A slightly more sophisticated 1-D model simulates unsteady-state flow conditions in river channels and solves cross-sectional averaged Saint-Venant equations to route the flow hydrograph and compute water surface elevation at each cross-section. There are some common 1-D models, such as HEC-RAS (USACE, 2016b) from U. S. Army Corps of Engineers, MIKE 11 (DHI, 2017a) from the Danish Hydraulic Institute.

1-D models are suitable for modeling hydraulic structures such as bridges, culverts, gated spillways, weirs, drop structures, as well as lateral structures (USACE, 2016b). However, they are not specialized for modeling 2-D features such as the spatial distribution of flows, meander, flooding in the catchment area.

2.1.2 2-D Hydrodynamic model

The 2-D hydrodynamic model solves depth-averaged mass and momentum equations to compute water-surface elevations and velocities at any point of used finite element grid. At each point, three values are computed including water depth, and velocities in two directions (i.e. *x* and *y* directions). The vertical accelerations of 2-D models are negligible. The velocity vectors are assumed to point in the same direction over the entire depth of the water column. There are some commonly used 2-D hydrodynamic models, such as

MIKE 21 (DHI, 2017b) from the Danish Hydraulic Institute, Delft3D (Deltares, 2017) from WL|Delft Hydraulics and Delft University of Technology, HEC-RAS 2D Modeling (USACE, 2016a) from U. S. Army Corps of Engineers. To implement a 2-D model, some typical data are required, such as bathymetric data, boundary conditions, and calibration data.

The most common boundary condition types of the 2-D model are water level at downstream and water discharge at upstream. Calibration data mainly based on point measurements of water level, velocity, and discharge. Various combinations were used, for example using only water level (Pham Van *et al.*, 2016; Ijaz *et al.* 2019), water level and discharge (Islam *et al.*, 2018; Xie *et al.*, 2019), water level and velocity (Zarzuelo *et al.*, 2019). These measurements are compared with model computations, and the parameters of the model are adjusted to improve the match of its results and measured values. Spatial calibration was also considered due to the complexity of river flow; however, recently spatial calibration was restricted in using velocity data along only one cross-section besides other data (Elias *et al.*, 2012).

The accurate description of river bathymetry is an important factor in the accuracy of the 2-D model. The river bathymetry represents the spatial variations in the riverbed by specifying the bed elevation at every node of the finite element grid of the computational domain. 2-D models were also found to be very sensitive to river bathymetry (Bovee, 1996). Therefore, the accuracy of the 2-D model is highly dependent on the accuracy of river bathymetry and the characteristics of the used finite element grid.

2.1.3 3-D Hydrodynamic model

3-D model is similar to the 2-D model, except that the governing equations are not depth-averaged. The number of layers in the water column is defined as the third dimension or vertical dimension (z) of the model besides the two horizontal dimensions (x and y). Hence, the 3-D model is suitable to describe the vertical profiles of flow and velocity as stratification, diffusion, and dispersion processes throughout the modeled area. The 3-D model thus consumes more computational time and requires more storage volume than the 2-D model. However, with the development of computer technology today,

computational time and storage volume may not be a big concerning issue with the 3-D model.

The 3-D model requires similar input data to the 2-D model. However, the measurements of velocity fields in the vertical direction are necessary for open boundary conditions and calibration of models (Fissel *et al.*, 2002). The accuracy of the river bathymetry is also an issue of the 3-D model.

2.1.4 The applications of hydrodynamic models

Hydrodynamic models hold a crucial role in investigating fluvial processes such as sediment transport, morphological changes, bank erosion, salinity intrusion, or flooding and risk. The followings are some selected studies related to these applications.

Coupling with sediment transport and morphological model, the hydrodynamic model is a very convenient process-based method to study sediment transport and morphological changes. The 2-D model is commonly coupled with sediment transport and morphological model to simulate the transport of cohesive/non-cohesive suspended sediment and/or morphological changes in river channels or coastal regions (van der Wegen *et al.*, 2011; Bi and Toorman, 2015; Xie *et al.*, 2018), the morphodynamic response of a tidal estuary inlet to sea-level rise (Yin *et al.*, 2019). The 3-D model is also coupled with sediment transport and morphological model to investigate sediment dynamics and morphodynamic changes in the estuaries and coastal zone (Thanh *et al.*, 2017; Tu *et al.*, 2019). Key factors that strongly influence the distribution and transport of suspended sediment, erosion/deposition patterns were investigated.

Hydrodynamic models are also useful for simulating riverbank erosion. The 1-D model and sediment transport model was coupled with a 2-D model of groundwater flow and a riverbank erosion model for investigating the mechanism of the cantilever failure of a composite riverbank (Deng *et al.*, 2019). The 2-D model and sediment transport model was coupled with groundwater flow and bank stability analyses to access the influence of hydraulic erosion on mass failure processes (Rinaldi *et al.*, 2008), with a process-based bank stability model to predict bank retreat (Lai *et al.*, 2015), or with geotechnical and vegetation module to simulate the riverbank erosion (Rousseau *et al.*, 2017).

Both 2-D and 3-D hydrodynamic models are applied to study salinity intrusion, but 3-D models are more common because of the capacity of describing detailed flow information. Thanh *et al.* (2017) and Tran Anh *et al.* (2018) successfully simulated salinity concentration in the Hau River (Vietnam), focusing on the salinization-prone section between Can Tho, Dinh An, and Tran De estuaries by coupling the 2-D model with salinity transport model. Besides, the 3-D model was also successfully combined with the salinity transport model to analyze the characteristics of salinity intrusion (Jeong *et al.*, 2010) or to quantify the influences of sea-level rise on saline water intrusion (Hong and Shen, 2012; Chen *et al.*, 2016).

A 2-D hydrodynamic model is also a good tool for investigating storm surge or flooding and risk. The 2-D model could be regularly incorporated with a wave model to simulate cyclones and analyze the attenuation role of mangroves within coastal environments (Rahdarian and Niksokhan, 2017), estimate hydrodynamic and morphological responses of the long-narrow estuary to a major storm (Kuang *et al.*, 2020). The 2-D model is also applied to assess the flood regulation function of paddy fields (Hai *et al.*, 2006), or investigate the local amplification of flow velocity in narrow river channel which is helpful information in evaluating flood/inundation risks in urban areas in the VMD (Takagi *et al.*, 2016b). The 1-D model is also used to analyze the characterization of the historical flood hazard, vulnerability, and risk and forecast the future hazard due to the projected sea-level rise in the VMD (Van *et al.*, 2012; Tri *et al.*, 2013).

2.2 Hydrodynamic models of tidal rivers using Riemann Boundary

As mentioned above, the upstream open boundaries of 2-D/3-D hydrodynamic models of rivers are commonly configured using measured river discharge. However, modeling works are often experienced with insufficient historical discharge data problems, so it is hard to describe an upstream open boundary of the flow model. Takagi *et al.* (2019) introduced a simplified methodology for modeling the flow of a large tidal river without discharge at the upstream boundary; the driving force is mainly produced by the variation of ocean elevation at the downstream open boundary. In this simplified model, the upstream boundary was applied to a Riemann Boundary, which enables progressive waves to pass through the boundary without reflection. The Riemann Boundary was also

demonstrated that it is convenient for setting up the upstream boundaries of not only river channels but also small tributaries (Takagi *et al.*, 2016b).

2.3 River topography interpolation

2.3.1 Bathymetric survey

Sciortino (2010) referred to a bathymetric survey as a hydrographic survey that measures the water depth of the river or ocean to produce the bathymetric map. In this activity, two measurement works are implemented simultaneously, including vertical depth and horizontal position measurements. These measurements can be supported by either manually (low tech, low cost) or sophisticated depth and position equipment (high tech, high cost), depending on the purpose of the survey. The vertical depth can be measured by a simple engineering echosounder or an advanced echosounder which can communicate with computer software to record the water depth data as ADCP, single or multibeam Sound Navigation And Ranging (SONAR) devices. The horizontal positions can be collected by various methods such as a floating line, theodolite, a Global positioning system (GPS), or a differential GPS (DGPS). ADCP devices are suitable for surveying the river cross-sections. SONAR devices are very convenient for the bathymetric survey, very high-resolution output data can be exported directly into the bathymetric map of the river or ocean. However, SONAR devices are suitable for large and relatively deep rivers.

Nowadays, many remote sensing techniques have been preferred for bathymetric mapping as Airborne bathymetric LiDAR (Hilldale and Raff, 2008), spatial depth, and through-water photogrammetry (Shintani and Fonstad, 2017). These methods allow a rapid survey of large areas and can be operated over a wide range of water depths in clear water, but their operations are strongly affected by various environmental factors such as water clarity, surface waves; the surveying cost is also very high because these devices must be mounted on planes or helicopters (Kasvi *et al.*, 2019).

Hydrographic data was measured and stored in different ways such as cross-sectional, random, zigzag, or very high-resolution distribution depending on the purposes or applying methods of the measurement works. Cross-sectional distribution is the most

common distribution of hydrographic data because it can describe effectively the anisotropy of riverbed. However, the distance between adjacent measured cross-sections should be close together to provide adequate information about the bottom features of the interested rivers, the recommended distance is 0.5 or 1 times the average river channel width to ensure that the interpolated bathymetry can capture sufficient major topographic features (Conner and Tonina, 2013).

2.3.2 Bathymetric interpolation

Bathymetric data play an important role in the 2-D/3-D flow model which shows detailed information of riverbed. Estimating river channel topography has been concerned by researchers in recent years. More than 40 different spatial interpolation methods were investigated and classified into two main groups including deterministic and geostatistical methods (Li and Heap, 2008). The deterministic interpolators estimate the value of unmeasured location by mathematical functions on the surrounding measured values. The interpolators, such as Triangular Irregular Networks (TIN), Inverse Distance Weighting (IDW), Radial Basis Function (RBF), and Local Polynomial Interpolation (LPI) are classified as deterministic methods. Conversely, the geostatistical methods apply both mathematical and statistical models that describe autocorrelation or statistical relationships between different measured points. Kriging interpolators were known as geostatistical methods.

The anisotropy of riverbed is very important information in interpolating the river bathymetry (Burroughes *et al.*, 2001; Goff and Nordfjord, 2004). This is a crucial viewpoint of customized or modified interpolation methods. Modified interpolation methods are commonly applied to IDW than other methods because it is simpler to implement. Burroughes *et al.* (2001) developed a zonal inverse distance weighting (Z-IDW) which recognizes and separates the estuary into some different zones based on the depth range to specify inverse distance weighting for each area separately. Modifying the searching method to consider the anisotropy of river channels is another approach to customize the IDW method. Merwade *et al.* (2006) introduced an elliptical inverse distance weighting (E-IDW) which involved measurement samples by an elliptical box followed the flow direction in a flow-oriented (s, n) coordinate system instead of a circular box to include the anisotropic nature of the channel while interpolating the river channel

bathymetry. Similarly, Andes and Cox (2017) applied a rectangular box followed the flow direction to define the rectilinear IDW (R-IDW) method. These modified interpolators indicated the ability to improve the estimated bathymetry of rivers.

Ordinary Kriging (OK) method is also applied to interpolate the river channel bathymetry. Carter and Shankar (1997) found that the OK method is unable to handle a trend in the data and suggested that the dominant trend should be removed from measured data before applying OK interpolator. Merwade *et al.* (2009) suggested a method to estimate the surface trend of the river bottom and remove it before making interpolation; this trend, finally, was added back to the estimated result to obtain the final bathymetry. This method improved significantly the estimated river topography.

2.4 Demand for deploying a 2-D flow model and estimating river bathymetry from sparse depth data for small tidal rivers in the VMD

Although the 2-D hydrodynamic model only estimates the depth-averaged velocity of a river, it is very effective to investigate the mechanism of most of the fluvial processes as sediment transport, riverbank erosion, riverbank retreat, salinity transport, storm surge, or flooding and risk. A 2-D model is also easy to upgrade to a 3-D model by adding vertical layers and collecting water velocity over the water column. Hence, modeling the 2-D model of a small tidal river is the first crucial step before investigating the mechanism of other fluvial processes to deal with related problems.

In the VMD, besides the large river system, most of the small tidal rivers are almost lack of hydrodynamic data so the simplified methodology of Takagi *et al.* (2019) is very helpful to conduct their 2-D flow models. However, this method is still in its infancy because it neglects some important characteristics affecting hydraulics in the estuarine environment. Further improvements should be considered to make this method more reliable and applicable to the small tidal rivers in the VMD.

The modern techniques are difficult to apply for surveying the topographic data of small tidal rivers in the VMD because they are generally deep and have very high turbidity. Although the ADCP-based method is also facing many dangers as the high speed of water flow, obstacles from fishing activities, or heavy traffic conditions in some rivers; it is the

most suitable method to apply in the VMD. However, the surveying boat should be tried to follow other strategies that are more flexible and faster than the cross-section strategy to be suitable for the local conditions in the VMD.

Many interpolation methods have been concentrated on improving the quality of river topography by involving the anisotropy of the riverbed. Most studies mainly deal with meandering and applied on cross-sectional data; lack of studies concentrated on other kinds of topographic data such as zigzag distribution data or improving the estimated depth at near riverbank areas which are important for studies as riverbank erosions or riverbank failures. Therefore, new interpolation methods that can be applied to zigzag data and improved the estimated depth near riverbank areas are really helpful for studying the small tidal rivers in the VMD.

Chapter 3 Interpolation of the river bathymetry based on sparse depth data

A Curvilinear search method is proposed as an interpolation search method for reproducing a three-dimensional river shape with sparse zigzag depth data. This method, combined with IDW, OK, and RBF interpolation, is optimal for estimating 3-D river shape from sparse zigzag depth data. It is excellent in shape estimation near the riverbank, especially in curved areas.

3.1 Introduction

Bathymetric data play an important role in river numerical modeling works. Most of the small tidal rivers in the VMD are lack of bathymetric data. Deploying modern equipment as LiDAR or remote sensing technology to measure high-resolution depth data to export directly the bathymetry might be difficult because rivers in this region are generally deep and have very high turbidity. The literature review in the previous chapter indicated that many studies have focussed on improving the quality of interpolated bathymetry by taking the anisotropy of riverbed into account. However, these studies mainly applied to cross-sectional or random distribution data which are difficult to measure in the VMD because of high water speed, heavy traffic load, and many obstacles from the fishing systems of local people. Hence, other kinds of depth data as zigzag data should be considered to make the field works easier in the VMD.

Estimating unmeasured depth locations by involving samples along the flow direction is the common solution to consider the anisotropy of the riverbed (Merwade *et al.*, 2006; Andes and Cox, 2017). As stated in the literature, E-IDW and R-IDW are operated in (s, n) coordinate system to deal with meandering rivers and data-point anisotropy. These methods worked effectively with rivers whose widths are not complex and distances between adjacent cross-sections are short (i.e. 0.5 or 1 times the average river channel width as mentioned by Conner and Tonina (2013)). If the distances between two adjacent become larger or rivers are not straight (i.e. in flow-oriented (s, n) coordinate system), the searching boxes (ecliptical or rectilinear box) of these methods unfollow the flow direction when finding the samples near the riverbank areas. Therefore, the estimated

depth near the riverbank, in this case, will be under-estimated. Hence, a new searching method should be proposed to account for this problem and optimize the near riverbank estimated topography.

Thalweg-line-based interpolations are other methods that effectively coped with riverbed anisotropy. Caviedes-Voullième *et al.* (2014) used the thalweg and two bank lines as break-lines to generate the interior splines parallel to the main flow direction and the depths along them are estimated by the linear method. Chen and Liu (2017) also manipulated three break-lines to distinguish the river channel but into four separated regions before resampling existed cross-sections and estimating extra cross-sections by various interpolators. Similarly, Lin *et al.* (2018) also divided the river into two regions by the thalweg and applied linear methods to estimate extra points for measured cross-sections and un-measured depths in the longitudinal direction. These interpolation methods obtain good estimation; however, the thalweg line is only specified effectively by cross-sectional data with short adjacent distances. Consequently, these methods are difficult to apply with sparse cross-sections or zigzag distribution data because it is difficult to estimate the thalweg line from them.

Zigzag distribution data are uncommon in river topography investigation because they are unable to describe well the transverse profiles of rivers and has many large areas lack of depth information. Krüger *et al.* (2018) proved that surveying strategies or sampling methods have a great influence on the quality of the interpolation results, and zigzag distribution data are also suitable for estimating the river topography. However, in this work, the zigzag data in double and ideal distribution were exported from very high-resolution data. In the VMD, most rivers are very deep, high flow speed, high traffic load, having many obstacles from fishing activities of local peoples so the zigzag strategy should be applied to measure the topographic data because it is very flexible and easy to operate in comparing with cross-sectional strategy.

In this study, the zigzag strategy was applied to acquire the hydrographic data of the study river and a new searching method was proposed to estimate the bathymetry from these measured depth data. The proposed searching method was guaranteed that involved samples follow the longitudinal direction regardless of the distance from the interpolation

location to them, estimating depth in the middle of the river or near the riverbanks. The proposed method was also compared with other searching methods by applying them with three common interpolators, including IDW, OK, and RBF method. Estimated bathymetries were also carefully compared to figure out which methods are suitable for similar studies in the future. All tasks in this study have been implemented on the Matlab environment instead of a geographic information system (GIS) software and output bathymetries could be directly applied for modeling the 2-D/3-D flow model of rivers by using Delft 3D software.

3.2 Methodology and data

3.2.1 Depth samples data

Exported depth samples from ADCP data by using WINRIVER II software are referred on the water-surface elevation. The water-surface elevation must be converted to the Vietnam National Datum (VN-2000) by using the nearest data contributed by the local government. Figure 3-1 shows the procedure jointing the VN-2000 water level at Station A with ADCP depth data to produce the VN-2000 discrete depth samples. In the procedure, the spatial distribution of water level across My Thanh River is assumed to be constant and equals with the water level at this station.

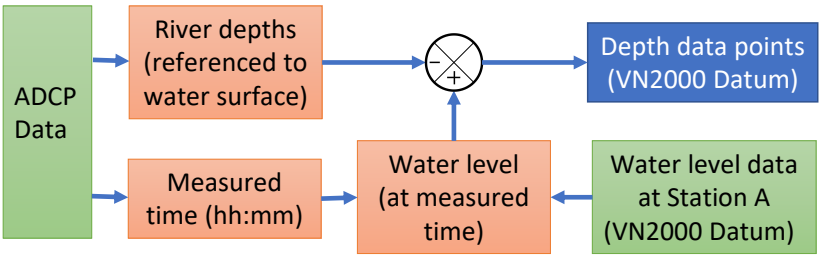

Figure 3-1. Convert ADCP data to depth samples.

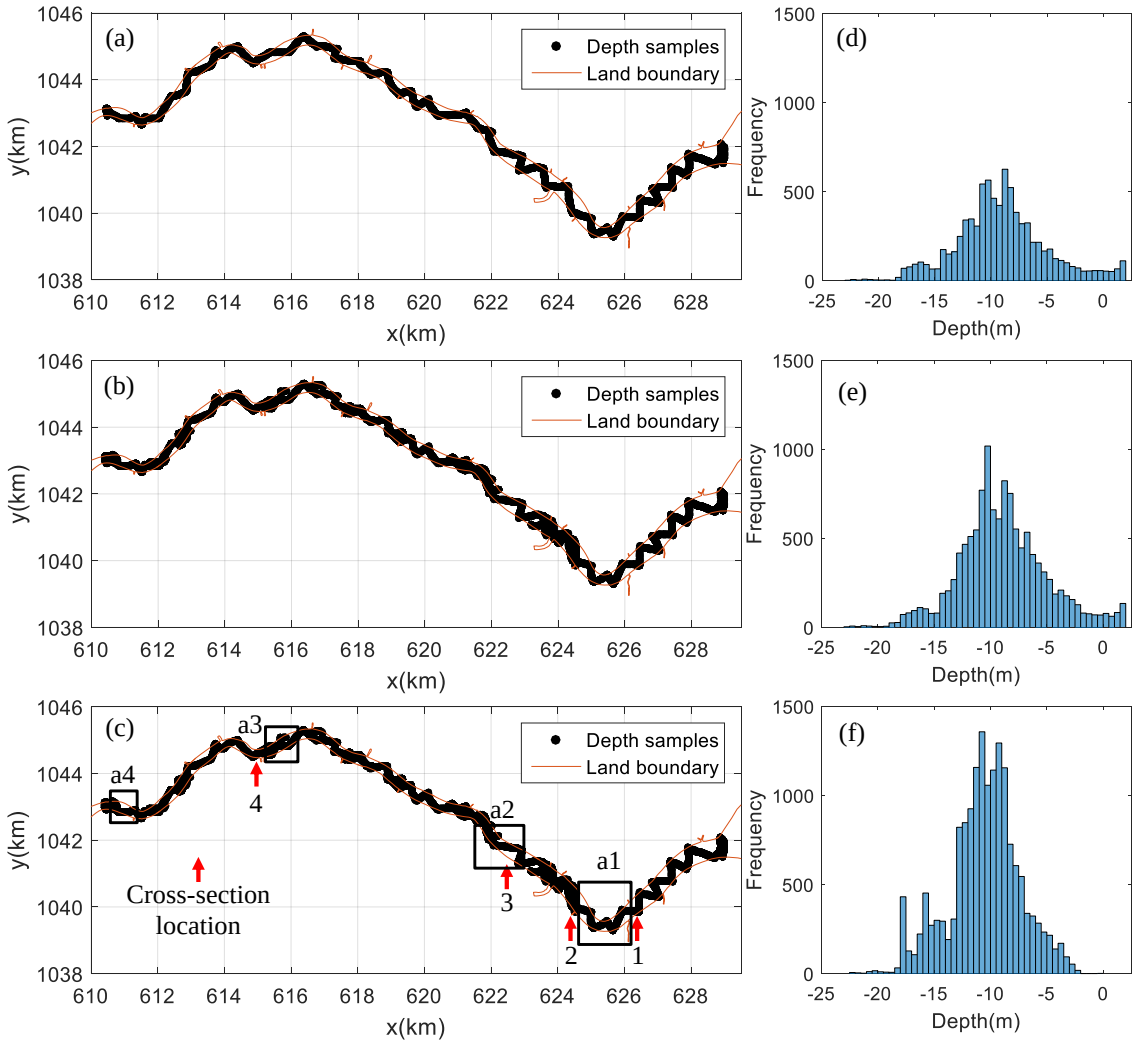

Figure 3-2. Distribution of classified depth sample data: calculating data (a, b) and calibrating data (c, d); and histogram graphs of their depth (c, d, f).

The depth samples in June with some selected samples in August were applied for interpolation study. The combination data were split into two groups, including calculating data for estimating the river bathymetry and testing data for validating applied interpolators. The calculating data are divided into two sub-groups, including (1) only zigzag samples (Figure 3-2 (a)), and (2) zigzag samples with some additional samples (Figure 3-2 (b)); the testing data include spatially distributed and four cross-sectional samples as shown in Figure 3-2 (c). The histograms of these groups show that the common depth of My Thanh River is about 11 m, with the deepest location is about 23 m (Figure 3-2 (d), (e), (f)).

3.2.2 Searching methods

The elliptical search (Merwade *et al.*, 2006) and rectilinear search (Andes and Cox, 2017) were improved the estimated river bathymetry significantly. However, these methods only work effectively with rivers which are nearly constant in width. In the case of river width highly changes, both elliptical and rectilinear search will have a common problem as shown in Figure 3-3. Obviously, in-stream samples at A in Figure 3-3 and near riverbank samples B will be included for interpolating at an in-stream unknown depth location C. This will generate more errors due to the certain change of the depth along the river cross-section. The searching box in this case has also not followed the river flow. To account for this problem, a new searching strategy was implemented as illustrated in Figure 3-3. This method works directly with the curvilinear grid of the study area in (x, y) Cartesian coordinate system. Figure 3-3 shows that the depth at the current grid node (*i*th, *j*th) is calculated by using depth samples on the left and the right of this node. These samples were found by sliding a searching box to both sides of the current node. The size of the box can be defined by users. The red curvilinear box in Figure 3-3 represents the trajectory of curvilinear search near the riverbank and in the area where river channel width changes significantly. Curvilinear search can be applied to derive new modified versions of common interpolation methods as IDW, OK, and RBF, so-called C-IDW, C-OK, and C-RBF (i.e. C stands for the Curvilinear search), respectively, for estimating riverbed topography using a sparse zigzag or cross-sectional dataset. Besides, the rectilinear search and the nearest neighbor search were also applied with these methods to derive six other methods including R-IDW, R-OK, R-RBF, NN-IDW, NN-OK, and NN-RBF with R and NN are represent for rectilinear and the nearest neighbor searches, respectively. All interpolators were applied to estimate the bathymetries of My Thanh River using the zigzag dataset to find out the suitable methods.

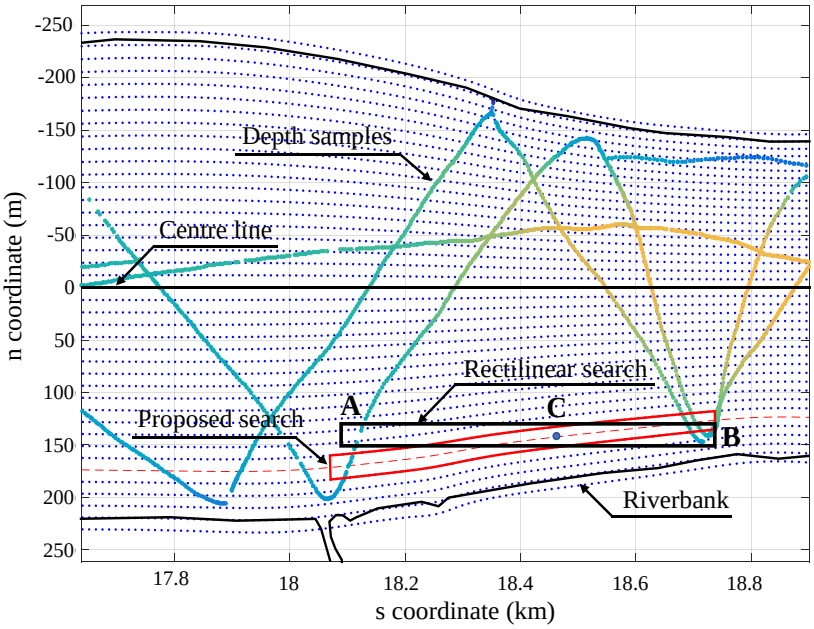

Figure 3-3. Previous and proposed searching methods.

3.2.3 Interpolation methods

IDW is a well-known deterministic interpolation method that can estimate the value of an unsampled location by a linear combination of involved samples (Li and Heap, 2008). The distances from involved samples to the unknown location are put in evaluating the impact of their values to the interpolated result by the following equation:

$$\hat{z}(x_0) = \frac{\sum_{i=1}^{N}(d_i^{-p} z(x_i))}{\sum_{i=1}^{N} d_i^{-p}} \quad (1)$$

where $\hat{z}(x_0)$ denotes the estimated value at an unknown location x_0, $z(x_i)$ is the value at the *i*th location, *N* is the number of included samples, d_i is the distance between x_0 and x_i, and *p* is the weighting power.

Similar to IDW, the RBF method also use the distances from included samples to interpolated location. However, RBF is a radial basis function network (RBFN) using these distances as inputs of its activation function to estimate the value of an unsampled location (Lin and Chen, 2004). The activation function is a nonlinear function that is radially symmetric in the input space. The RBF estimator equation as following:

$$\hat{z}(x_0) = \sum_{i=1}^{N} w_i \varphi(\|x_0 - x_i\|) \quad (2)$$

with w_i is the weight coefficients computed by solving the following linear system:

$$\begin{bmatrix} \varphi(\|x_1 - x_1\|) & \varphi(\|x_2 - x_1\|) & \cdots & \varphi(\|x_N - x_1\|) \\ \varphi(\|x_1 - x_2\|) & \varphi(\|x_2 - x_2\|) & \ldots & \varphi(\|x_N - x_2\|) \\ \vdots & \vdots & \ddots & \vdots \\ \varphi(\|x_1 - x_N\|) & \varphi(\|x_2 - x_N\|) & \ldots & \varphi(\|x_N - x_n\|) \end{bmatrix} \begin{bmatrix} w_1 \\ w_2 \\ \vdots \\ w_N \end{bmatrix} = \begin{bmatrix} z(x_1) \\ z(x_2) \\ \vdots \\ z(x_N) \end{bmatrix} \quad (3)$$

where $\varphi(r) = \varphi(\|x_i - x_j\|)$ is the activation function. There are many kinds of activation functions such as the thin-plate-spline function, the Gaussian function, the multiquadric function, and the inverse multiquadric function (Chen *et al.*, 1991). In this study, however, only the multiquadric function was applied, its formulation as following (σ is a constant):

$$\varphi(x_i - x_j) = \sqrt{1 + \frac{(x_i - x_j)^2}{\sigma^2}} \quad (4)$$

The OK method is a kind of geostatistics interpolator estimated the unknown value by using the spatial correlation between collected samples (Li and Heap, 2008), the OK estimator equation as following:

$$\hat{z}(x_0) = \sum_{i=1}^{N} \lambda_i \, z(x_i) + [1 - \sum_{i=1}^{N} \lambda_i] \mu(x_0) \quad (5)$$

where λ_i is Kriging weights and $\sum_{i=1}^{N} \lambda_i = 1$, and $\mu(x_0)$ is the local mean of samples within the search box. The Kriging weights are computed by the following linear system:

$$\begin{bmatrix} C(x_1, x_1) & C(x_1, x_2) & \cdots & C(x_1, x_N) & 1 \\ C(x_2, x_1) & C(x_2, x_2) & \ldots & C(x_2, x_N) & 1 \\ \vdots & \vdots & \ddots & \vdots & \vdots \\ C(x_N, x_1) & C(x_N, x_2) & \cdots & C(x_N, x_N) & 1 \\ 1 & 1 & \cdots & 1 & 0 \end{bmatrix} \begin{bmatrix} \lambda_1 \\ \lambda_2 \\ \vdots \\ \lambda_N \\ \mu(x_0) \end{bmatrix} = \begin{bmatrix} C(x_0, x_1) \\ C(x_0, x_2) \\ \vdots \\ C(x_0, x_N) \\ 1 \end{bmatrix} \quad (6)$$

where C is a covariance function describing the spatial correlation between referenced samples, and C is calculated from the semivariogram model of samples.

3.2.4 Implementation of interpolation methods

Most procedures in this study were developed in a Matlab environment. Figure 3-4 describes the algorithm of the MATLAB program which follows several steps. At first, the curvilinear grid of My Thanh River was created separately by using the RGFGRID tool (Deltares, 2020b) and converted to Matlab structure data by using the QuickPLOT tool (Deltares, 2014b). This structure data contains the (x, y) Cartesian coordinates of the computational grid where the depths will be estimated. Next, the structure data and all kinds of depth samples were imported to Matlab as input data. After that, all searching methods were used to find samples for interpolating the depth at the current grid node (*i*th, *j*th). The IDW, RBF, and OK methods were implemented based on the equation (1), (2), and (3), respectively. The RBF and OK method applied exist MATLAB libraries which were developed by Chirokov (2006) and Ramm (2011), respectively. Ramm (2011) developed this library mainly based on the Gstat package (Pebesma and Wesseling, 1998). However, IDW was written by the author it is easy to implement. The mean absolute errors (MAEs) of predicted bathymetries were calculated to access the quality of output bathymetries. If MAEs of any methods are large, the parameters will be modified and run the program again. No specific criteria for MAEs, the try-and-error method was applied to reduce the errors as much as possible. Finally, the final bathymetries will be exported into the DEP-extension file (Deltares, 2014a), which are ready for 2-D/3-D flow modeling.

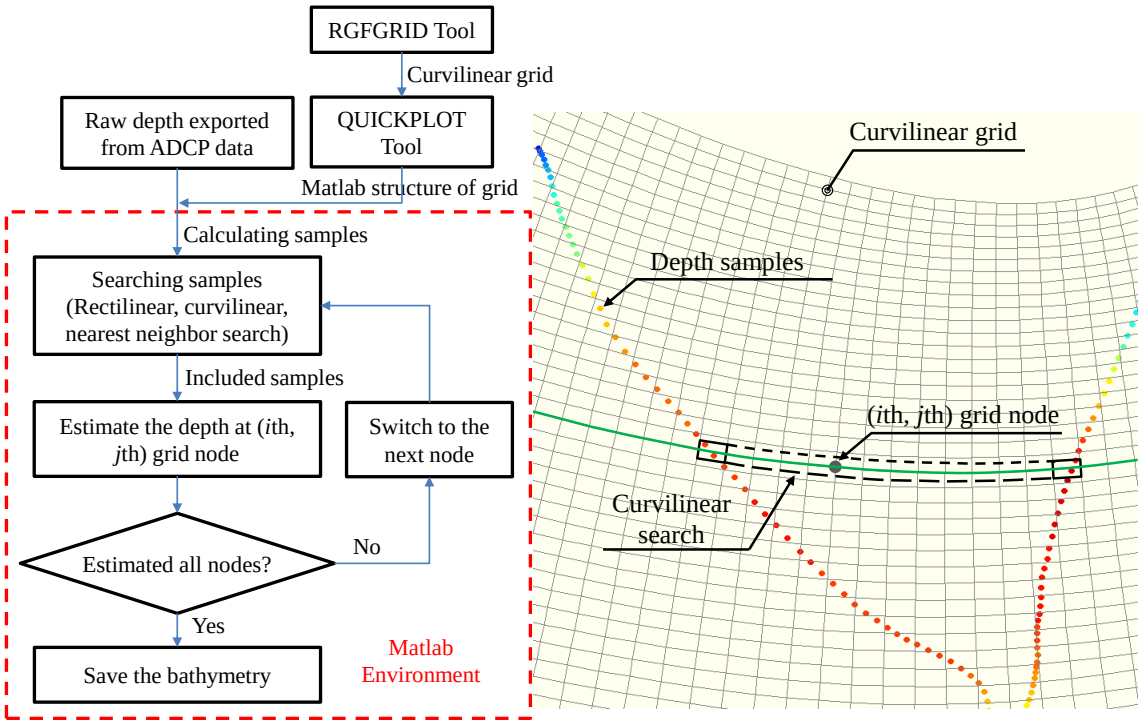

Figure 3-4. Flowchart of interpolation Matlab program.

3.3 Results and discussions

3.3.1 Comparing surfaces

To assess the influence of samples density and determine which interpolation methods are suitable with the zigzag dataset, the MAE between estimated bathymetries and testing dataset (Figure 3-2 (e)) were calculated by the following equation:

$$\mathrm{MAE} = \frac{1}{\mathrm{N}}\sum_{i=1}^{N}(\hat{z}_i - z_i) \qquad (7)$$

where N is the number of testing depth samples, $\hat{z}_i$ and z_i are the estimated and measured depth at the ith location, respectively.

The MAE values of estimated bathymetries shown in Table 3-1 indicate that NN-IDW, NN-OK, and NN-RBF method resulted in a large discrepancy from the testing data (greater than 1 m), while C-IDW is the best suitable method with the lowest MAE values in both cases of testing data. Additionally, with the same interpolators, curvilinear search

always generated better bathymetry than others. It means that curvilinear search is the most suitable searching method working with the zigzag distribution samples. Moreover, increasing the density of samples the predicted bedforms were improved, and it is an unsurprising result because more samples caught more bottom features; this is consistent with the study of Diaconu *et al.* (2019) instead of differences in the spatial distribution of samples.

Table 3-1. Calculated MAE of estimated bathymetries.

MAE (m)	Calculation cases	
Interpolation methods	Case 1	Case 2
C-IDW	0.60	0.55
C-OK	0.70	0.65
C-RBF	0.61	0.56
R-IDW	0.63	0.59
R-OK	0.81	0.73
R-RBF	0.77	0.68
NN-IDW	1.58	1.46
NN-OK	1.19	1.17
NN-RBF	1.21	1.11

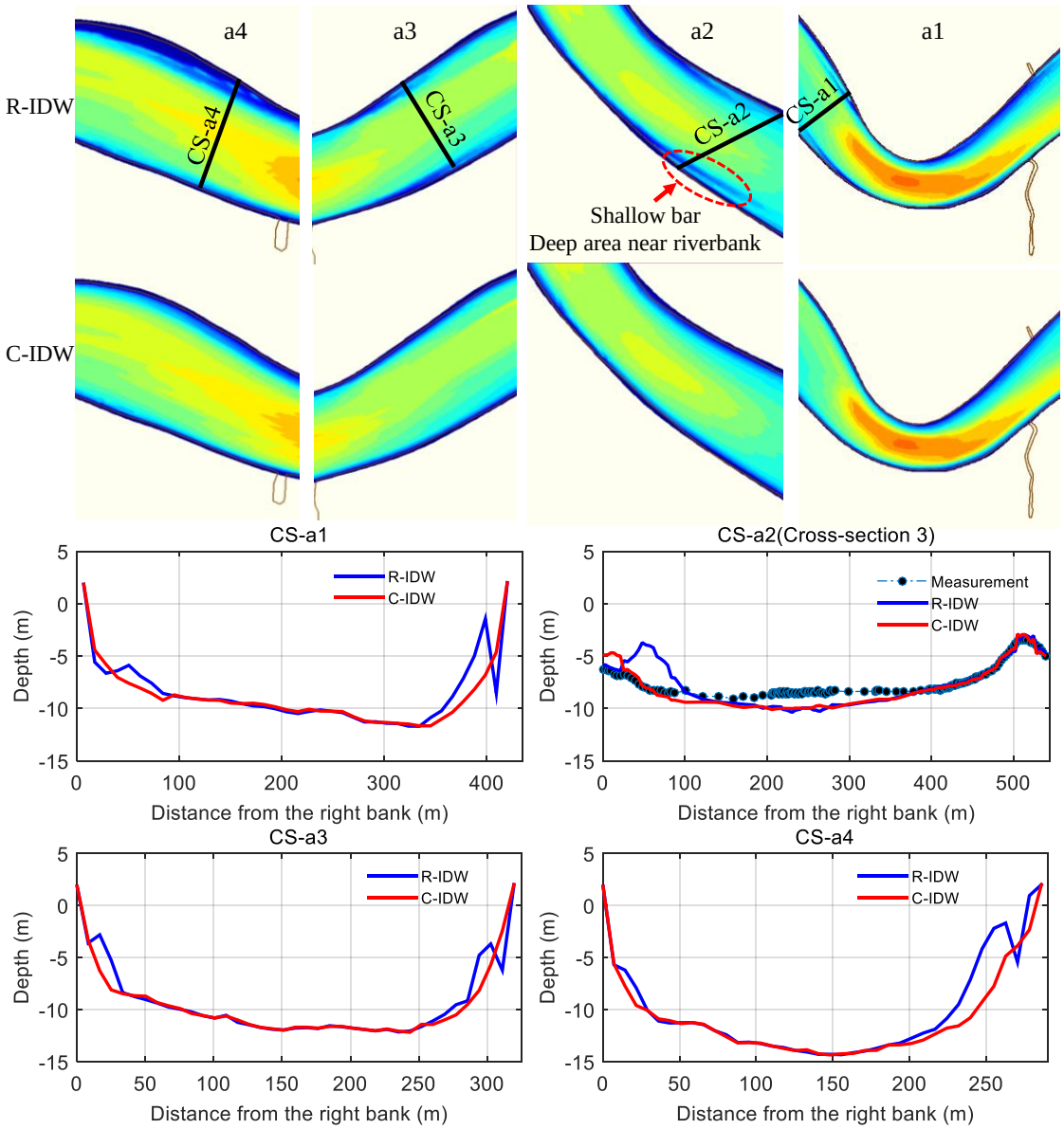

Figure 3-5. The estimated depth of C-IDW and R-IDW interpolator at four areas marked from a1 to a4 in Figure 3.2, and extracted depth profiles of four selected cross-sections from CS-a1 to CS-a4 in these areas. In the case of CS-a2, its location is near Cross-section 3, so the estimated depths were extracted at the measured locations.

To present the problem of rectilinear search at the near riverbank, four potential areas in the My Thanh River were selected and marked from a1 to a4 as shown in Figure 3-2(c). The estimated bedforms of these areas are displayed in Figure 3-5, the first row and second row were estimated by R-IDW and C-IDW, respectively. The bedforms in the first row look abnormal and unnatural; the shallow bars and deep areas near riverbanks are the results of involving unsuitable depth samples for interpolating. Similarly, the R-OK

method also has the same problem with R-IDW because the OK method also manipulated directly the depth values, while the RBF method used the distances. Nevertheless, the bedforms estimated by C-IDW are very smooth and natural. Hence, the curvilinear search has already improved the estimated bathymetry but mainly in near-bank regions, while the middle area is very consistent with R-IDW. Exported cross-sectional profiles of CS-a1 to CS-a4 are clearly to show that C-IDW cross-sections are very smooth in comparison with R-IDW cross-sections.

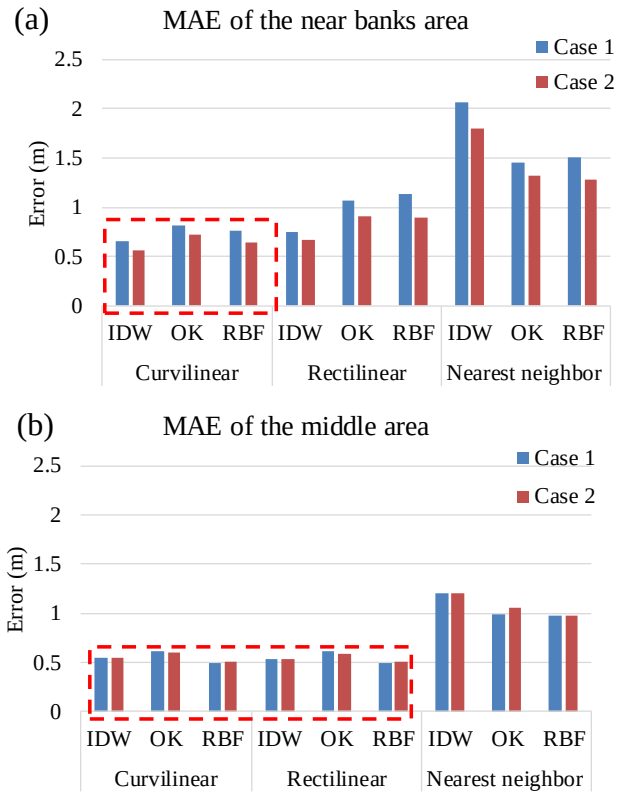

Figure 3-6. The regional MAEs of using interpolators calculated at near riverbank areas (a) and the middle area of the river (b), the red-dash boxes show the suitable interpolators in this region.

However, the regional MAEs calculated by estimated bedforms and testing data reveals other interesting results. Adding more samples has only refined the estimated depth at the near riverbank areas, the MAEs notably decreased in all cases (Figure 3-6 (a)), while slightly changed in the middle of the river (Figure 3-6 (b)). Figure 3-6 indicates that C-IDW, C-OK, R-IDW, and R-OK methods are suitable to reproduce the depth of the middle river, while only C-IDW and C-OK are suitable for the near riverbank areas.

Consequently, two groups of interpolation methods can be applied to predict the river bedform based on zigzag depth samples. The first group is the interpolators working with curvilinear search (C-IDW, C-OK, C-RBF) and R-RBF method. C-IDW is the best method. The second group is regional interpolators which are the C-IDW method for estimating the near riverbank areas combining with C-RBF or R-RBF method for estimating the middle river area, respectively.

3.3.2 Comparing cross-sections

The error of estimated depth was calculated by the following equation

$$e_i = \hat{z}_i - z_i \quad (8)$$

where, $\hat{z}_i$ and z_i are the estimated and measured depth of the *i*th sample. Figure 3-7 illustrates the error profile of four selected cross-sections named from 1 to 4 as shown in Figure 3-2 (c). Especially, Cross-sections 1 and 3 are situated in areas a1 and a2 where the estimated bathymetries generated R-IDW method has a problem, therefore they are effective to compare the performance of interpolation methods. Generally, the primary differences occur at near riverbank areas except Cross-sections 2 and 3 where the OK method has larger errors in the middle. The interpolation methods working with curvilinear search could generate a better cross-sections profile than them working with rectilinear search except for the IDW and RBF method at Cross-section 2 and Cross-section 4, respectively (Table 3-2). The mean MAEs show that C-IDW is the best method.

Particularly, interpolation methods worked with rectilinear search reconstructed worse depths at the left bank and the right bank of Cross-sections 1 and 3, respectively, than with curvilinear search; it reconfirmed the drawback of the rectilinear search. Located in the straight river where the topography is not significantly changed, the depth profile of Cross-section 2 was estimated well, but the R-OK method underestimated the depth near the left bank. It may be occurred by the semivariogram model was not described well the spatial correlation in this area. The depth profile of Cross-section 4 is the most difficult to predict, especially at the left bank, because it is located at a complex meandering where the topography is rapidly changed. No methods operated well at this bank except the C-IDW.

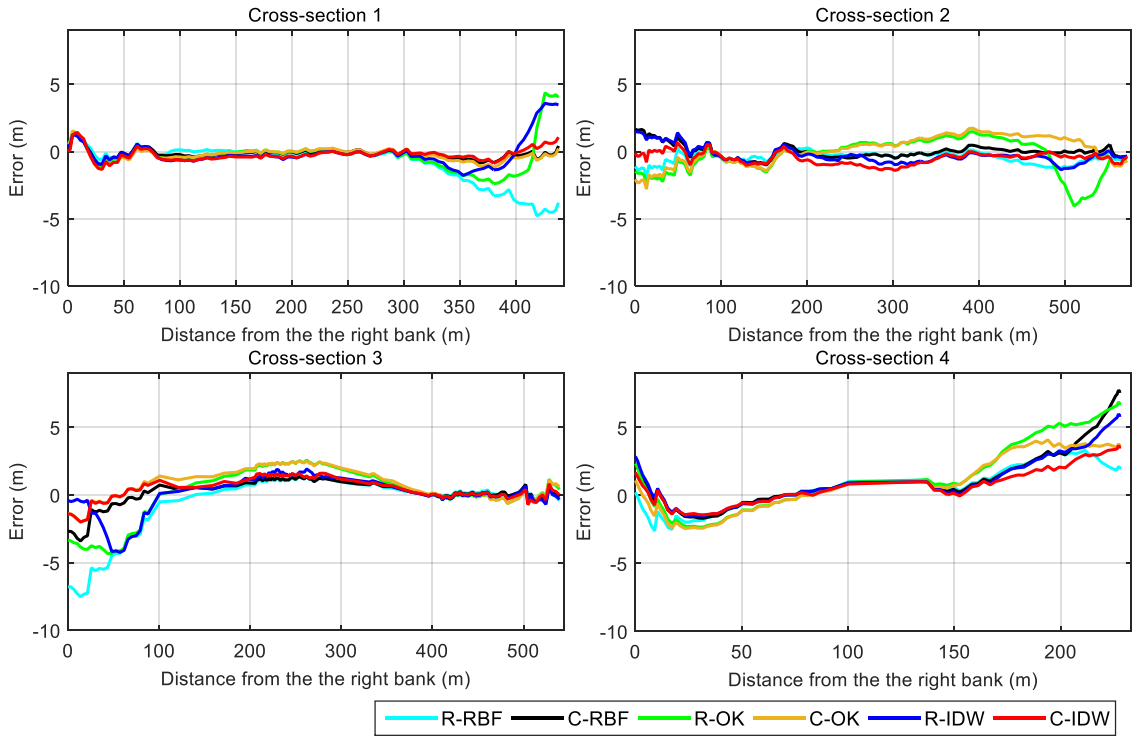

Figure 3-7. Error profiles of estimated depths by applied interpolators at four cross-sections, their locations are marked in Figure 3-2.

Table 3-2. Calculated MAE of four reproduced cross-sections.

MAE (m)	Cross-section 1	Cross-section 2	Cross-section 3	Cross-section 4	Mean MAE
C-IDW	0.28	0.54	0.88	2.77	1.12
R-IDW	1.12	0.53	1.78	5.84	2.32
C-OK	0.28	1.04	1.95	6.65	2.48
R-OK	1.29	2.05	3.75	11.40	4.62
C-RBF	0.17	0.75	1.00	8.19	2.53
R-RBF	2.76	4.97	5.28	3.19	4.05

3.3.3 Discussions and future works

The demand for estimating an accurate bathymetry has been remained because of the crucial role of bathymetric data in the numerical model. This study not only indicated the effectiveness of curvilinear search but also figured out the suitable methods which can work well with the sparse depth dataset collected by zigzag strategy. This is a fast, flexible, easy-to-setup strategy, and very convenient to apply for rivers in the VMD.

Difficulties of estimating depth for the near-bank regions are mainly caused by insufficient depth data (Andes and Cox, 2017; Hilton *et al.*, 2019). Hilton *et al.* (2019) suggested using modern equipment (i.e. ATLAS, LiDAR, ICESat-2) to collect more data. However, these systems might be not operated well with rivers in the VMD because of the deep and high-turbidity water. So, the proposal of the curvilinear search is the first step to improve the estimated depth of these areas. Besides, our study also ensures that the predicted bathymetry is ready for flow modeling. The main factor to have this ability is that our algorithm used directly the computational grid of the numerical model. Andes and Cox (2017) and Hilton *et al.* (2019) concluded that their output bathymetries were also ready for flow modeling, but they did not clearly show how to archive this. However, our method has only validated with the curvilinear grid, other types of the grid such as unstructured grid or grid from other numerical tools should be supported in the future.

Similar to the cross-section strategy, the zigzag strategy also can not measure the depth of the near riverbank areas because of the limitation of the navigation. To deal with this handicap, the riverbank elevations at the land boundary were assumed 2 m (VN-2000 datum). After that, additional samples were generated at some locations where have the shortest distance to the riverbank by using the linear method. This method was already applied by Falcão *et al.* (2016) to combine the estimated river bathymetry and floodplain area. However, it is better to find a new way to estimate the bathymetry for these areas in the future, such as analyzing the satellite images, drone-based remote imaging at the lower-low-water (LLW) period of the tide, scanning depth by a sonar sensor, or generating depth by combining the cross-section tendency and small random-depths represented for the roughness of the riverbank.

Our interpolation results revealed that the depth of the middle river is estimated easier than that of near-bank areas, it is consistent with the results of Andes and Cox (2017) and Hilton *et al.* (2019). It implies that a mixed-method joining between methods operated well in the near-bank and methods worked well in the middle river areas should be applied to have the best bathymetry. This study already proposed such kind of methods. However, the frontier between the near-bank and middle areas where is the most effective, or how to create a suitable grid should be also considered to generate a more exact bathymetry. Furthermore, the influences of other properties of the zigzag route should be carefully analyzed to suggest a good measurement strategy, such as the wavelength, waveform as the study of Krüger *et al.* (2018), or locations of the zigzag routes which might catch more bottom features.

3.4 Conclusions of river bathymetry interpolation using sparse depth data

The searching methods play an important role in riverbed interpolation, especially in the case of using a sparse depth dataset. The curvilinear search made the estimated bathymetry smoother and more exact than other recent searching methods. The results show that C-IDW and regional interpolation methods are suitable with a zigzag dataset. However, more studies should be conducted in the future to further refining the estimated bathymetry, such as find out a good planning zigzag measurement strategy, improving measurements in the near riverbank regions, and supporting more grid types.

Chapter 4 Practical flow modelling of a small tidal river with insufficient hydrodynamic information

When applying the 2-D flow model, the Riemann boundary condition proposed by Takagi *et al.* (2019) is improved by considering the flow velocity loss near the riverbank, and the boundary condition at the upstream end is given.

4.1 Introduction

Two types of open boundary conditions have been applied to the 2-D/3-D flow model. The first is water open boundary condition located at downstream to generate the water level variation. This boundary condition can be configured by using time-series water level or tidal constituents which were obtained by conducting harmonic analysis on tidal data. The second is the discharge boundary condition situated upstream of the rivers. Commonly, discharge data were measured during the field measurement works, and long-period data are not available in most cases. In fieldwork, river discharge is measured by the ADCP device. Many factors affect the measurement results of ADCP as water turbidity, mud layer on the riverbed, or weather condition. The biggest problem is that ADCP is operated by humans so measuring continuously in the long-period is a difficult task. Hence, lack of or insufficient discharge data is one of the common problems in configuring the upstream open boundary conditions of the 2-D/3-D flow model.

To account for this problem, Takagi *et al.* (2019) proposed a simplified method to implement the 2-D flow model of a tidal river in the VMD which requires no discharge data for upstream open boundary conditions. In this method, the upstream boundary has remained as an open boundary with the Riemann Boundary setting which permits progressive waves to pass through the boundary without any reflection. The downstream boundary condition was applied to tidal constituents to generating ocean tides. The velocity of this model was adjusted by the Manning's *n* value. The simulation results show that this method could reproduce very good water levels and velocities of the tidal river. However, the effect of upstream discharge in the rainy season must be eliminated from hydrodynamic data before applying this method. Besides, the Riemann Boundary is

one-dimensional, the velocities of this boundary are inversely proportional with the river depth (Deltares, 2017), near upstream boundary velocities at both banks will be very large because of shallow depths. This may cause the instability of the numerical model and should be solved. A method to correct these velocities will improve significantly the estimated flow fields of the river of interest.

My Thanh River is a small tidal river in the VMD that fully under the effect of the tidal regime of the East Sea. Although the tidal data at My Thanh station have been only available until 2007, the ocean tides in 2018 can be predicted by the tidal constituents. Hence, in this study, the simplified model proposed by Takagi *et al.* (2019) could be applied to conduct the 2-D flow model of My Thanh River and the drawback of normal Riemann Boundary was solved by introducing an extended Riemann Boundary. The proposed boundary also enables using the measured depth-averaged velocities over the upstream cross-section of the study area to calibrate the parameters of the model to cope with the lack of calibration data.

4.2 Materials and methods

4.2.1 Hydrodynamic data

Ocean tides were collected by the water level gauge at Tidal data at My Thanh station from 1985 to 2007. These data were manipulated to analyze the tide regime to prove that the sea-level in the East Sea is rising. It is easy to see the discrepancy between observed and tidal harmonic analysis data as shown in Figure 4-1 (a). This may be caused by the seasonal variation of water level at My Thanh gauge. Obviously, the water level is increasing sharply in the rainy season started in June and decreasing slightly in the dry season started in the early of January (Figure 4-1 (b)). This variation is mainly affected by Bassac River discharge because the difference between gauge data and analysis data is so large (about 0.5m), so only discharge from My Thanh River is difficult to make this difference. However, more investigation should be conducted to confirm this statement. The data also unveiled that the sea-level has increased about 20cm over 23 years (from 1985 to 2007) (Figure 4-1 (c)). Sea-level is increasing and will be faster in the future (Takagi *et al.*, 2019). Besides, the tidal data can be also used to analyze the tidal

constituents using the harmonic analysis tool of Delft 3D software. This tool applied the following equation (Deltares, 2020a)

$$H(t) = A_0 + \sum_{i=1}^{k} A_i F_i \cos\left(\omega_i t + (V_0 + u)_i - G_i\right) \quad (9)$$

where *H(t)* denote the water level at time t, A_0 is the mean water level at a certain period, k is the number of constituents, *A* is the astronomical amplitude of a constituent, *F* is nodal amplitude factor, ω is angular velocity, $(V_0 + u)$ is the astronomical argument, and *G* is improved Kapa number or local phase lag. At a specific tidal station, A_0, A_i, and G_i can be estimated by the above equation using a least mean squares analysis. Consequently, if for a specific tidal station, A_0, A_i, and G_i are known, the water level *H(t)* can be predicted at any time. Hence, by knowing the tidal constituents, the long period flow model can be very easy to implement.

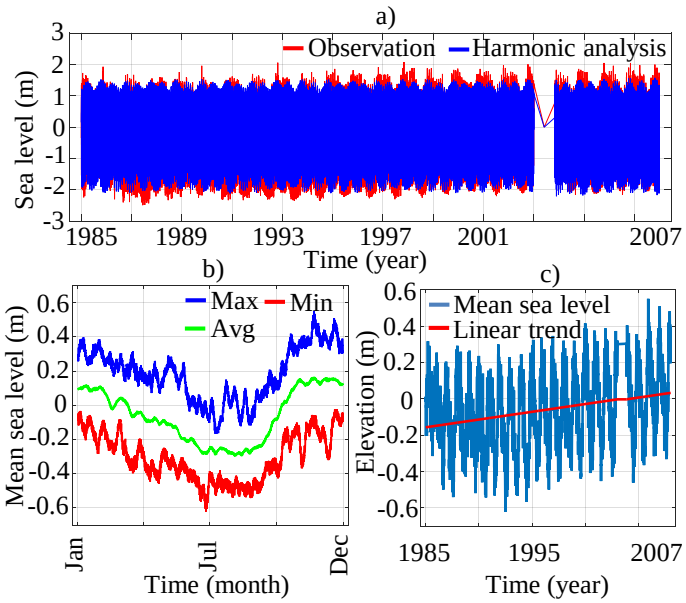

Figure 4-1. Tidal data analysis: observation and harmonic analysis (a); max, min, and average values (b); and mean sea-level and linear trend (c).

The field measurements on 28th and 29th August 2018 were used for calibrating the parameters of the proposed 2-D flow model, including water levels at upstream (Station B), downstream (Station A), and depth-averaged velocities over the upstream cross-section (Figure 4-2). The graph in Figure 4-2 (b) shows the water levels at Station B after

removing their mean because the national datum is not available at this location. The water levels at Station A are referred on national datum VN-2000 and only available during the measurements of depth (Figure 4-2 (b)). The mean velocities over the upstream cross-section (Figure 4-2 (c)) can not be used for calibrating the parameters of the flow model because upstream is located in the upstream open boundary of the flow model. However, the modeling method in this study enabled using them for flow model calibration.

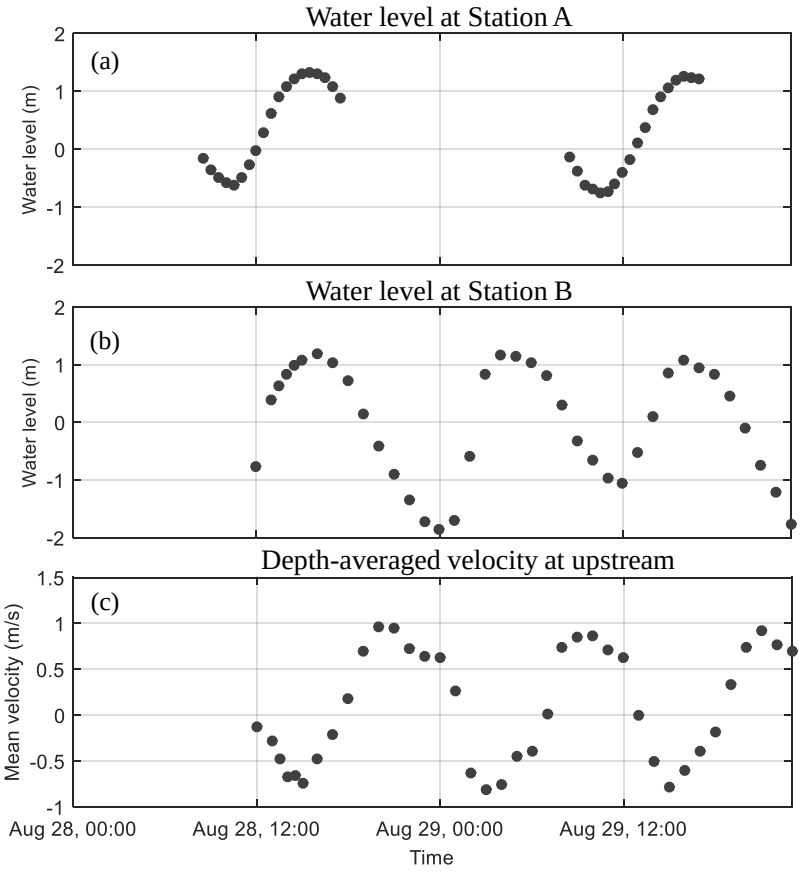

Figure 4-2. Field data measured on 28th and 29th August 2018.

4.2.2 Mathematical of the hydrodynamic model

To model the 2-D numerical flow for My Thanh River, the Navier Stokes equations for an incompressible fluid based on the shallow water and the Boussinesq assumptions were solved by the Delft3D-FLOW software, developed by Deltares (Deltares 2014a). The depth-averaged continuity equation of the model is derived by integration of the

continuity equation for incompressible fluids ($\nabla.\vec{u} = 0$) over the total depth, taken into account the kinematic boundary conditions at the water surface and bed level, and is given by:

$$\frac{\partial \zeta}{\partial t} + \frac{1}{\sqrt{G_{\xi\xi}}\sqrt{G_{\eta\eta}}}\frac{\partial((d+\zeta)U\sqrt{G_{\eta\eta}})}{\partial \xi} + \frac{1}{\sqrt{G_{\xi\xi}}\sqrt{G_{\eta\eta}}}\frac{\partial((d+\zeta)V\sqrt{G_{\xi\xi}})}{\partial \eta} = (d+\zeta)Q \qquad (10)$$

with *U* and *V* are the depth-averaged velocities

$$U = \frac{1}{d+\zeta}\int_d^\zeta u dz \qquad (11)$$

$$V = \frac{1}{d+\zeta}\int_d^\zeta v dz \qquad (12)$$

and *Q* denotes the contributions per unit area due to the discharge or withdrawal of water, precipitation, and evaporation:

$$Q = \int_{-1}^{0}(qin - qout)d\sigma + P - E \qquad (13)$$

ζ is water level above a horizontal reference (datum), *t* is time, *d* is the depth below the datum, *z* is the vertical coordinate in physical space, $\sqrt{G_{\xi\xi}}$ and $\sqrt{G_{\eta\eta}}$ are coefficients used to transform curvilinear to rectangular coordinates, *u* is flow velocity in the *x*- or ξ-direction, *v* is the fluid velocity in the *y*- or η-direction, *U* is the depth-averaged velocity in ξ-direction, *V* is the depth-averaged velocity in *y*- or η-direction, *qin* and *qout* the local sources and sinks of water per unit of volume, respectively, *P* is the non-local source term of precipitation, and *E* is non-local sink term due to evaporation.

4.2.3 Model setup

This study deployed 2-D shallow-water equation models built-in Delft3D software to reproduce the flow model of My Thanh River. The model was simulated in four days from 26th to 28th August 2018, comprising two days (26th and 27th) for "spinning-up" the flow model and two days for reproducing the river flow in the measurement period (28th and 29th). The computational domain is described by a curvilinear grid with a total of

81,360 nodes same of which was used to generate the river bathymetry. The minimum resolution of the grid was set to 5m. This model comprised two open boundary conditions (Figure 4-3 (a)). At the estuary, water level type boundary (Tide-BC) was applied with the value set by using tidal constituents because of Tide-BC located near My Thanh gauges. At the upstream, discharge data is only available in the measurement period and the quality is not good enough under the influence of surrounding disturbance such as heavy rain, high water turbidity. In case of insufficient upstream discharge data, the Riemann boundary condition, 1-D non-wave reflection condition, is a useful solution because it can replace the upstream discharge boundary (Takagi *et al.*, 2019). However, because of the omitting of discharge, Manning's *n* must be manipulated to calibrate the discharge or velocity results. In this study, Manning's *n* was chosen by using the try-and-error method. The parameters of the numerical flow model of My Thanh River were summarized in Table 4-1.

Table 4-1. 2-D flow model parameters

Parameter	Value
Time step (minute)	0.25
Initial water level (m)	0
Manning's *n* ($s/m^{1/3}$)	0.016-0.03
Horizontal eddy viscosity (m^2/s)	1

To solve the drawback of the normal Riemann Boundary, the solution is that the upstream boundary is straightly extended in the upstream direction about 22 km, and its bathymetry linearly changes from the upstream location and become unit depth cross-section at the new end (Figure 4-3 (b)). The constant depth of 10m was chosen for the new end. The Riemann Boundary applied at the new upstream is so-called "extended Riemann" (ext-Riemann) boundary and comprised two zero discharge open boundaries at both sides of the river (Discharge-BC1 and Discharge-BC2) and a zero Riemann Boundary at the middle (Riemann-BC1). In this study, the wave reflection property of the new boundary

is interpreted in a very simple way based on the length (L) of the Riemann boundary (Figure 4-3 (b)). Three properties of the wave reflection such as full, intermediate, and non-reflection are defined corresponding with L equals zero meters, nearly half of river width, and full river width.

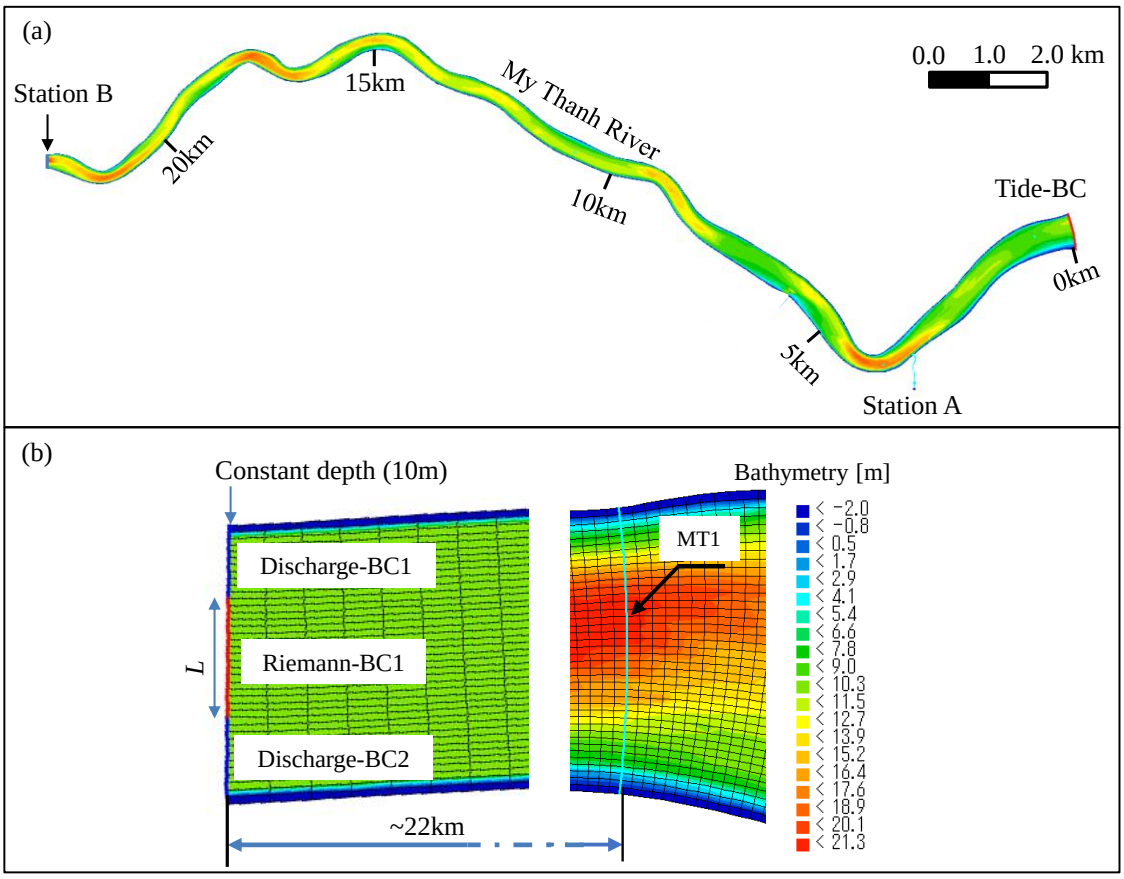

Figure 4-3. The 2D flow model of My Thanh River: the study area (a), the structure of the extended Riemann boundary.

4.3 Results and discussions

4.3.1 Numerical model results

Although downstream water levels are predicted by the historical tide from 1985 to 2007, the estimated levels are good agreement with the measured levels (Figure 4-1 (b)). However, some discrepancies are still exits. Water levels at Station A less depend on the wave reflection properties, this may cause by this station is very near downstream open boundary. Besides, estimated water levels at upstream (Station B) show a large

dependence on the wave reflection properties. Intermediate reflection generates the smallest water level amplitude (Figure 4-4 (a)), but it can reproduce the best upstream mean velocities in terms of amplitude and phase as illustrated in Figure 4-4 (c).

Table 4-2 shows the RMSE values of estimated values of water levels at Station A, Station B, and mean velocities over the upstream cross-section of the flow model in three simulation cases of wave reflection properties. These results indicate that Intermediate reflection is the best property of the ext-Riemann Boundary, it has the smallest RMSEs. Full and Non reflection could estimate good water levels; however, the upstream mean velocities show a large difference in phase, especially with Full reflection property.

Table 4-2. RMSE of flow model results in the case of changing the wave reflection property of the ext-Riemann boundary.

RMSE	Simulation case		
	Intermediate	Full	Non
Water level at Station A (m)	0.32	0.33	0.32
Water level at Station B (m)	0.32	0.30	0.38
Mean velocity at upstream (m/s)	0.25	0.38	0.39

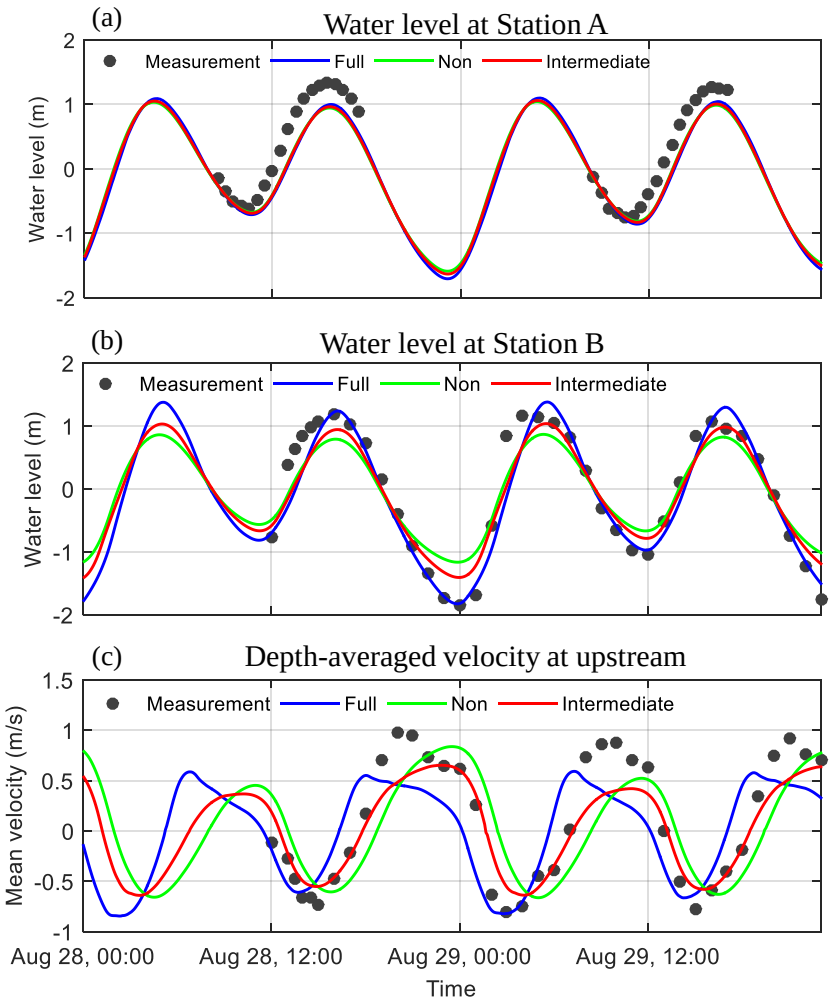

Figure 4-4. The simulation results of My Thanh River: Water levels at Station A (a), Station B (b), and depth-averaged velocities over the upstream cross-section (c).

Figure 4-5 (a) displays the spatial distribution of model velocity vectors around the upstream boundary at 23:00, 28th August 2018, in case of applying directly Riemann Boundary at the upstream location. Large velocity vectors show near both banks of the river caused by the disadvantage of the normal Riemann Boundary as mentioned in the previous section. Figure 4-5 (b) represents these velocity vectors generated by the proposed flow model with the ext-Riemann Boundary. It is obvious to recognize that the proposed flow model already eliminated the unusual velocity vectors around the upstream location.

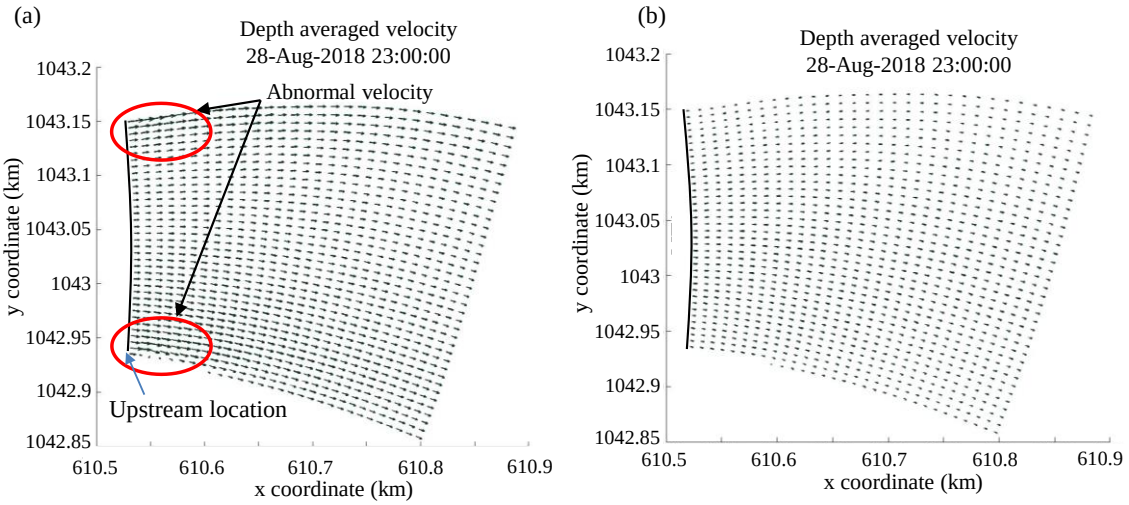

Figure 4-5. The spatial distribution of velocity vectors near the upstream cross-section: applied Riemann boundary at the upstream (a), extended Riemann Boundary (b).

4.3.2 Discussions and future works

This study introduced a method to simulate the flow of a small tidal river in the VMD with insufficient data. This method can be applied to investigate the flow of the small tidal rivers with only downstream tidal data as values for the downstream boundary, no required discharge data for the upstream boundary, and field velocity and water level data for calibrating the parameters of the model. The extended Riemann Boundary could solve the drawback in the method of Takagi *et al.* (2019), and the flow model in this study could estimate well the near riverbanks velocities around the upstream of the study area.

Besides, the proposed method enables using the least measured data for calibrating the parameters. Normally, to calibrate the parameters, at least one measurement station is required between the upstream and downstream locations to collect the water level and velocity. Takagi *et al.* (2019) used the measured water levels and velocities at Can Tho station to calibrate their model. However, the situation in this study is different, only the measured velocity at the upstream cross-section of the study area is available. In other words, the measured data are not sufficient for applying the 2-D flow model directly. Extended Riemann Boundary has not only improved the estimated velocities but also solved this insufficient data problem and reduced the measurements for similar works in the future.

Some remained problems should be considered to solve in future studies. The 2-D flow model has eliminated the vertical movement of the flow and salinity transport which play a crucial role in tidal rivers. The interaction between fresh-water and salt-water causing the vertical stratification of the river flow. The quality of the flow model should be significantly improved by involving these kinds of phenomena.

The simplified flow model applied in this study can not simulate the large effect of the upstream discharge. Takagi *et al.* (2019) removed the effect of upstream discharge in the rainy season from the measurement data before using for modeling by eliminating the mean values from measured water levels and velocities. The effect of the discharge from upstream of My Thanh River is minor so the simplified model suggested by Takagi *et al.* (2019) can be applied directly. However, a method to estimate the upstream discharge should further improve the flow field of My Thanh River. Moreover, small channels on both sides of rivers are also the special features of tidal rivers in the VMD. They can be natural or artificial channels and their widths are up to about one-third of the main rivers, so their flows should influence the main rivers. Their flow models should be conducted in future studies.

Although there are some remained problems, the proposed flow model has reproduced a reasonable flow field which is very helpful for other river-related studies in the future such as sediment transport, bed morphology development, salinity transport, or sea-level rise projection, and so on. The estimated flow fields near the riverbank provide useful data for investigating and predicting riverbank erosion, riverbank failures under different conditions of flow at some potential locations of the study rivers.

4.4 Conclusions of apply 2-D flow model for a small tidal river with insufficient hydrodynamic data

In this study, the most important result is that a suitable 2-D flow model was proposed for small tidal rivers with insufficient hydraulic data and easy to simulate in a long period. Additionally, this study found that the built-in Riemann boundary condition in Delft 3D is the main cause of the instability of the flow model because of unusual velocity near the boundary and suggested a solution to solve this. Although some improvements should be conducted, the proposed flow model will be very helpful for other river-related studies in

the future such as sediment transport, riverbed morphology development, riverbank erosions, riverbank failures, sea-level rise projection, and so on.

Chapter 5 The Improvements of 2-D flow model of small tidal rivers in the VMD

The tidal data were reviewed using the yearly changes of the primary constituents, and the model structure was modified and optimized by estimating the upstream freshwater discharge and implementing the approximate flow model of a small channel to significantly improve the reproducibility of the flow field. The parameters of the new model were calibrated using the spatio-temporal velocity records measured by the ADCP device. It was shown that it was improved. From these, it is stated that the proposed method can reproduce the flow of a small tidal river for a long time relatively easily.

5.1 Introduction

The 2-D flow model of My Thanh River in Chapter 4 could estimate the flow field of a small tidal river using the least of field data. Although the estimated water level and velocity reasonably agreed with the measured data, the discrepancies between them have already remained. Some reasons can be explained these discrepancies. The flow model in Chapter 4 mainly calibrated Manning's *n* value and the length of ext-Riemann Boundary to adjust the river flows. However, rivers in the VMD are under the effects of freshwater discharge from natural channels, large rivers, and also from human activities as agriculture, aquaculture, and industry, so upstream discharge is important and needs to be considered to improve the quality of the estimated flows.

Besides, tributary effects causing by the small channels along the study river are commonly omitted because of insufficient related data. Rivers in the VMD have a lot of small natural and artificial channels located on both sides whose widths are up to one-third of the main river's width. So, they certainly influence the flows of the main rivers. In My Thanh River, Tra Nhieu channel is the largest channel located on the right bank and near the estuary, the depth around its mouth is about 6.5 m. The estimated bathymetry in Figure 5-3(c) shows the flow from this channel has made some scoured holes around the channel's mouth demonstrating that this channel strongly affects the flows of My Thanh River. However, the Tra Nhieu channel has not been implemented in the flow

model in Chapter 4. Hence, conducting the approximate model of this channel should be improved significantly the predicted flows of My Thanh River.

As mentioned in the literature in Chapter 2, most recent studies have calibrated their flow model mainly based on comparing computed and observed data at some fixed locations. Although Elias *et al.* (2012) already calibrated and validated their model by spatio-temporal data, they only considered the measured velocity along only one cross-section besides other data. One convenient feature of the ADCP device is that water velocity can be also measured during depth measurement, these velocity data describe well the flow field of the river in both the spatial and temporal domain. However, it is difficult to apply these velocity data for calibrating and validating the 2-D flow model because most of the hydrodynamic modeling tools only support storing calculation results at certain points or cross-sections. Putting a lot of observation points to obtain the model values of measured velocities is an ineffective method because a large number of velocity records were measured and they located around the river. Hence, finding the method to calculate the model results of these velocity records is very necessary for calibrating and validating the 2-D flow model using spatio-temporal data. Using the spatio-temporal velocity data for calibrating the model parameters should be better than using data at fixed locations because they represent well the flow field of the river.

This chapter aims to improve the 2-D flow model of My Thanh River in chapter 4 by considering upstream freshwater discharge and the tributary effect of small channels. To accomplish this goal, a method to calibrate the value of ext-Riemann Boundary to consider the upstream freshwater discharge was introduced and a simplified model of the small channel was proposed to consider the tributary effect of a small channel near the estuary of the study river. Parameters of the new 2-D model were calibrated by using fixed-location field data and spatio-temporal field data to closely consider the spatial changes of the flow field.

5.2 Methodology and data

5.2.1 Spatio-temporal velocity data

Spatio-temporal velocity data of My Thanh River were measured by the mounted-boat ADCP device during the river depth measurement period. At every location, besides the

depth, ADCP also measured the velocity information in the vertical direction of the water column. Spatio-temporal velocity has the same spatial and temporal distribution with depth data as presented in Figure 5-1. Containing the vertical information, these velocity data are very effective for calibrating the 3-D flow model.

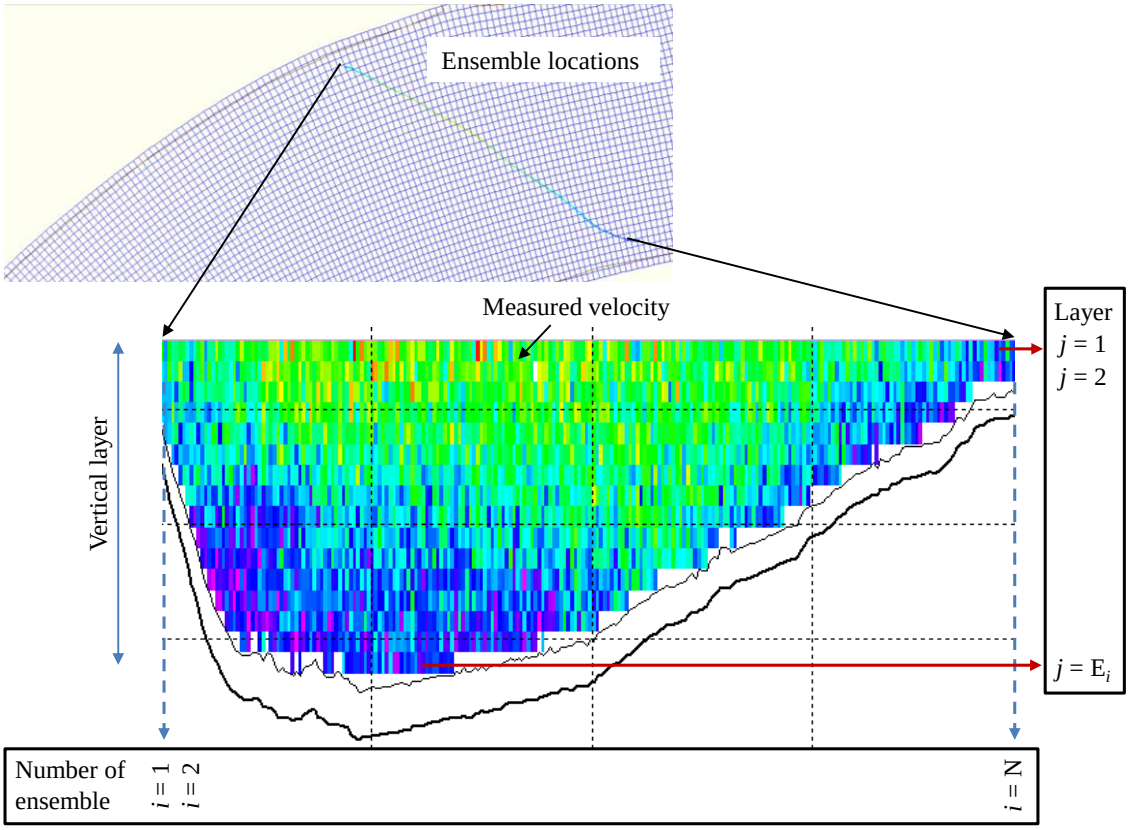

Figure 5-1. Distribution of velocity data measured by the ADCP device.

Figure 5-1 describes the spatial locations and vertical distribution of velocity data of one segment of ADCP data. One segment has measured N locations or N ensembles (i.e. the name in ADCP data), each location contains E_i layers and E_i value depended on the local depth. The different time between two adjacent ensembles is nearly two seconds. In this research, spatio-temporal velocity data were applied to calibrate the 2-D flow model of My Thanh River. The mean value of spatio-temporal velocity of every segment was calculated by the algorithm in Sect 5.2.4, so-called spatio-temporally depth-averaged velocity in this study.

5.2.2 Tidal data

The yearly change of the primary tidal constituents (M_2, S_2, K_1, and O_1) at My Thanh and Tran De station were analyzed and shown in Figure 5-2. The changing of amplitude and phase of the primary constituents from 1985 to 1990 are abnormal and unnatural, so these tidal data were eliminated from the harmonic analysis. Tran De station is located at the estuary of Hau River, about 10 km from My Thanh station, so the phase lag of tidal constituents at this station is different from them at My Thanh station as shown in Figure 5-2. Consequently, tidal data from 1991 to 2014 of both stations were applied to analyze the amplitude of tidal constituents, but only tidal data from 1991 to 2007 at My Thanh station were used to analyze the phases lag to guarantee the correctness of them. Table 5-1 indicates the changing of primary tidal constituents before and after reviewing the tidal data. The new constituents were applied to configure the value for the Tide-BC boundary of the 2-D flow model My Thanh River in this chapter.

Table 5-1. The changing of the primary tidal constituents at My Thanh station.

Constituent	Tide from 1985 to 2007		Tide from 1991 to 2014	
	Amplitude	Phase	Amplitude	Phase
M_2	0.85	75	0.89	72
S_2	0.27	124	0.32	121
K_1	0.53	342	0.58	334
O_1	0.38	276	0.40	284

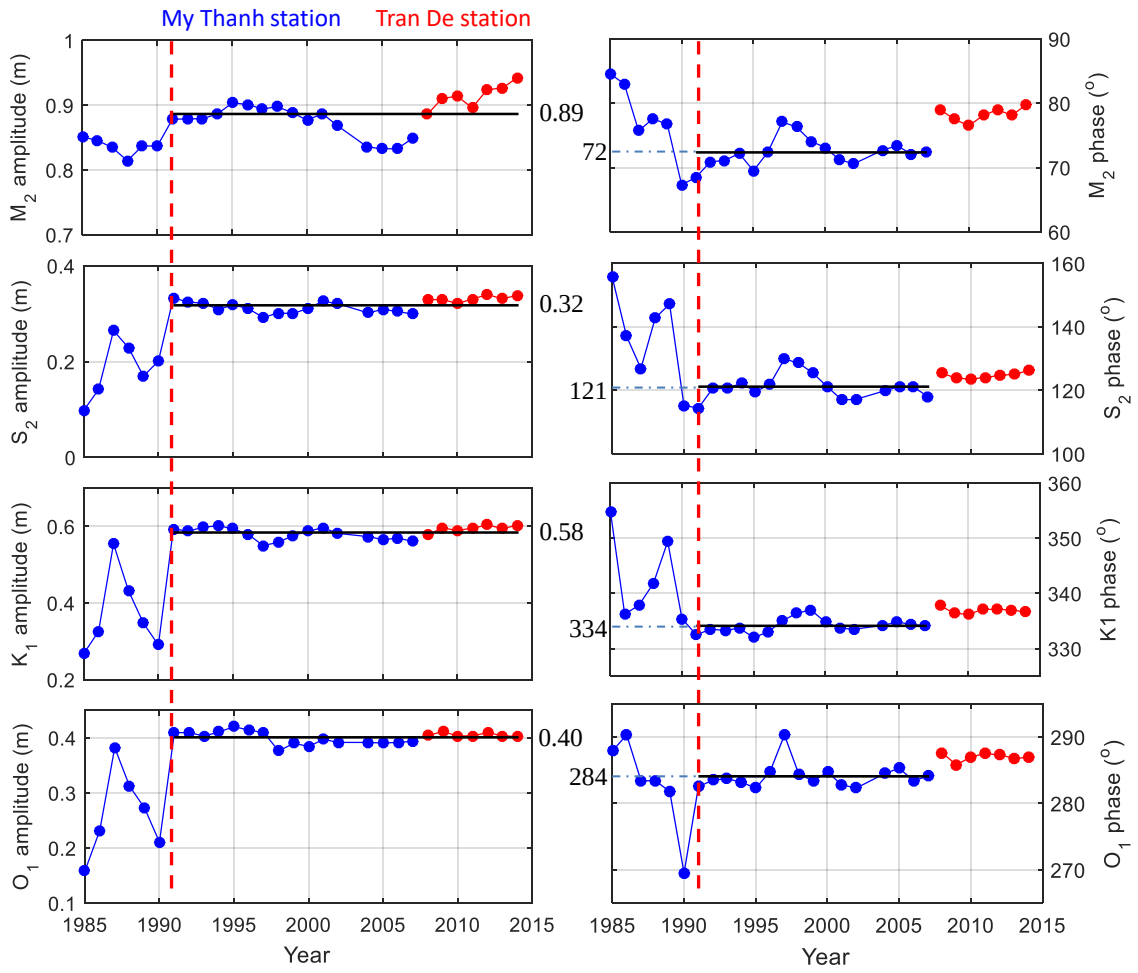

Figure 5-2. The yearly changing of amplitude and phase of the primary constituents of the tide at My Thanh and Tran De station.

5.2.3 Model setup

The model of this chapter is mainly based on the flow model in Chapter 4. In this chapter, Chapter 4's model was improved by considering two main factors, including upstream freshwater discharge, and downstream tributary. Figure 5-3 describes the structure of the new 2-D flow model of My Thanh River in this chapter. The main difference of this model compared with the previous model is the simplified model of Channel 2 which was applied to consider the tributary effect of Tra Nhieu channel. The primary parameters of the flow models in this chapter are described in Table 5-2.

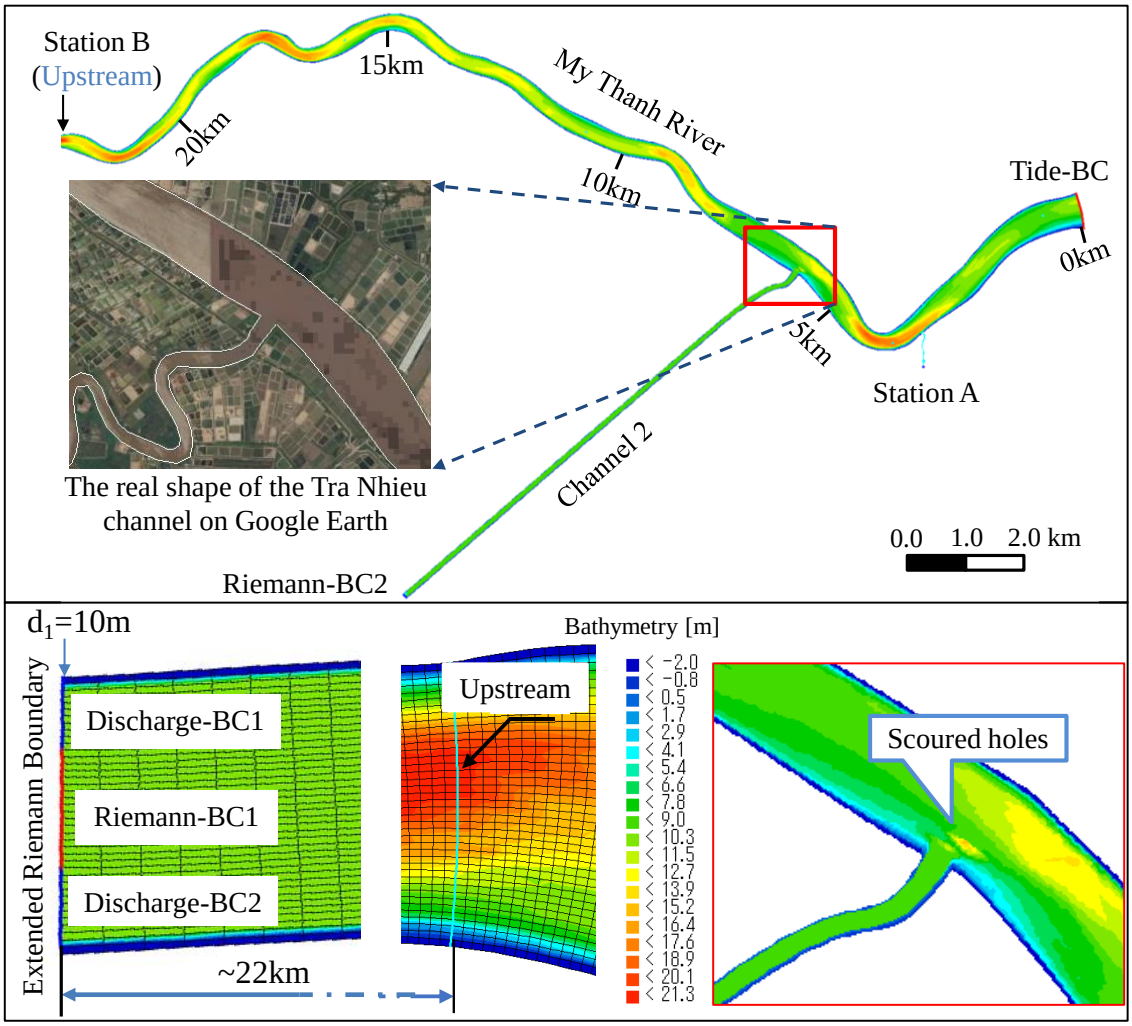

Figure 5-3. The new 2-D flow model of My Thanh River.

Table 5-2. Parameters of the 2-D flow model of My Thanh River in this chapter.

Parameter	New model
Time step (minute)	0.25
Initial water level (m)	0
Manning's *n* value of main river ($s/m^{1/3}$)	0.016 - 0.03
Manning's *n* value of Channel 2 ($s/m^{1/3}$)	0.04
Horizontal eddy viscosity (m^2/s)	1

5.2.3.1 Estimation of upstream discharge

The extended Riemann Boundary (Riemann-BC1) was configured with zero value, its estimated velocities are computed by the following equation.

$$u_1 = F_{R1}(t) - \zeta_1\sqrt{\frac{g}{d_1}} = -\zeta_1\sqrt{\frac{g}{d_1}} \quad (14)$$

where u_1 denotes the depth-averaged velocity in ξ-direction of Riemann-BC1, $F_{R1}(t)$ is the value of Riemann-BC1 (equals zero), ζ_1 is water level, g is the acceleration due to gravity, d_1 is water depth at Riemann-BC1 (d_1 = 10m). Equation (14) shows that the velocity of Riemann-BC1 only depends on water elevation (ζ_1) because g and d_1 are constants. The upstream-ward discharge in flood tide should be larger than it in neap tide because the area of the cross-section in flood tide is bigger than in neap tide. As a result, the cumulative discharge computed by equation (15) will have a negative value.

$$Q_{1cum} = \int_0^T Q_1 dt = \frac{1}{d_1+\zeta_1}\int_0^T \int_{d_1}^{\zeta_1} u_1 dz dt \quad (15)$$

where Q_{1cum} denotes the cumulative discharge of upstream after a specific simulation period *T (s)*. If the river is not under the effect of upstream freshwater discharge, the cumulative discharge after a simulation period (T) will fluctuate around the 0 m^3 value or average discharge ($\bar{Q}_1$) will approach 0 m^3/s. Hence, to make Q_{1cum} vary around 0 m^3, the average discharge at upstream calculated by equation (16) will be used to configure values for Discharge-BC1 and Discharge-BC2 but with opposite sign.

$$\bar{Q}_1 = \frac{Q_{1cum}}{T} \quad (16)$$

However, most tidal rivers in the VMD are under the effect of upstream freshwater discharge, the additional discharge will be added to Discharge-BC1 and Discharge-BC2 besides $\bar{Q}_1$ to represent the effect of the upstream freshwater discharge on the flow model. In this study, the mean value of the measured discharge in August 2018 was used.

5.2.3.2 Consideration of downstream tributary

The tributary effects of small channels along both sides of rivers are commonly omitted in flow modeling because of inadequate data. In My Thanh River, a small channel named Tra Nhieu (called Channel 2 in this chapter) was found on the right bank about 5 km from the estuary, its width at the mouth about 100 m, one-fifth of the main river. In chapter 4, the model of Channel 2 was not implemented because of the lack of all information. In this chapter, a simplified method was proposed to implement the approximate 2-D flow model of this channel. A straight canal about 10 km, the depth linearly increasing from 6.5 m at its mouth to 8.5 m at the in-land end was used to describe Channel 2. A Riemann Boundary named Riemann-BC2 was also applied to configure the open boundary condition of Channel 2.

The value of Riemann-BC2 was estimated by the following procedures. First, simulating the flow model with a zero value of Riemann-BC2. Next, calculating the mean model velocity $\bar{u}_2$ from the simulated cumulative discharge Q_{2cum} and the area of cross-section, and the mean model water level $\bar{\zeta}_2$ at this boundary. After that, the new mean value $\bar{F}_{R2}$ of Riemann-BC2 was calculated by using $\bar{\zeta}_2$ and $-\bar{u}_2$ using equations (17). Finally, simulating the model and compensating the value of $\bar{F}_{R2}$ to let the mean discharge at Riemann-BC2 approximately 0 m^3/s, similar technique with estimating the total discharge of Discharge-BC1 and Discharge-BC2. The effect of its upstream freshwater discharge was eliminated because the measured discharge data are not available.

$$\bar{F}_{R2} = \bar{u}_2 - \bar{\zeta}_2\sqrt{\frac{g}{d_2}} \tag{17}$$

here g and d_2 are gravitational acceleration and the depth at Riemann-BC2, respectively.

5.2.3.3 Model simulation cases

The 2-D flow model of My Thanh River in Chapter 4 was improved in this chapter by reviewing the tidal data, considering the upstream discharge and downstream tributary effect of the small channel. A total of six simulation cases were conducted as described in Table 5-3 including Case 0 is the Intermediate wave reflection case in Chapter 4. The results of Case 0 are manipulated as a reference for the improvement in this chapter. Case

1 is used to simulate the model after reviewing the tidal data at My Thanh station and nearby station. Cases 2 and 3 are applied to consider the effect of upstream discharge on the model. Cases 4 and 5 are deployed to calibrate the approximate 2-D flow model of Channel 2 and investigate the changes in the flow field after adding it.

Table 5-3. The simulation cases.

Case	Tide-BC	Discharge-BC1 (m^3/s)	Discharge-BC2 (m^3/s)	Riemann-BC2 (m/s)
Case 0	Old tide	0	0	-
Case 1	Modified tide	0	0	-
Case 2	Modified tide	110	110	-
Case 3	Modified tide	250	250	-
Case 4	Modified tide	250	250	0
Case 5	Modified tide	250	250	-0.23

5.2.4 The algorithm to estimate the model result of spatio-temporal velocity

The spatio-temporal velocity of My Thanh River was also measured by ADCP during depth measurement. Figure 5-1 indicates the general distribution velocity data of one specific segment of zigzag data of ADCP. At every segment, ADCP recorded *N* ensembles of water velocity, each ensemble contains E_j layers and the number of layers depends on the river depth. These measured data are very useful for calibrating the 2-D/3-D flow model.

To be convenient for calibrating and validating the flow model, the spatio-temporal velocity data were divided into small groups; ensembles collected continuously in 5 minutes were be classified into the same group. The spatio-temporally depth-averaged velocity (V_{sda}) of each group was calculated by the following equation:

$$V_{sda} = \frac{1}{N}\sum_{i=1}^{N}\left[\frac{1}{E_i}\sum_{j=1}^{E_i} v_{ij}\right] \quad (18)$$

where N indicates the number of ensembles in a group, E_i is the number of valid layers at ith-ensemble, v_{ij} is the velocity of jth-layer of ith-ensemble.

Figure 5-4 presents the algorithm to calculate V_{sda} for measurement and computation velocity. First, exporting necessary raw measurement data, such as the coordinates, velocity in vertical layers, and measured date/time, from ADCP data. After that, removing invalid ensembles and layers and classifying them into separate groups based on date/time information. Next, calculating the depth-averaged velocity at every ensemble of each group, and interpolating their computed values by four nearest computed values of grid cell containing them which were found by a cell-searching algorithm. Finally, calculating the mean values of each group to obtain the measurement and computation values of the spatio-temporally depth-averaged velocity.

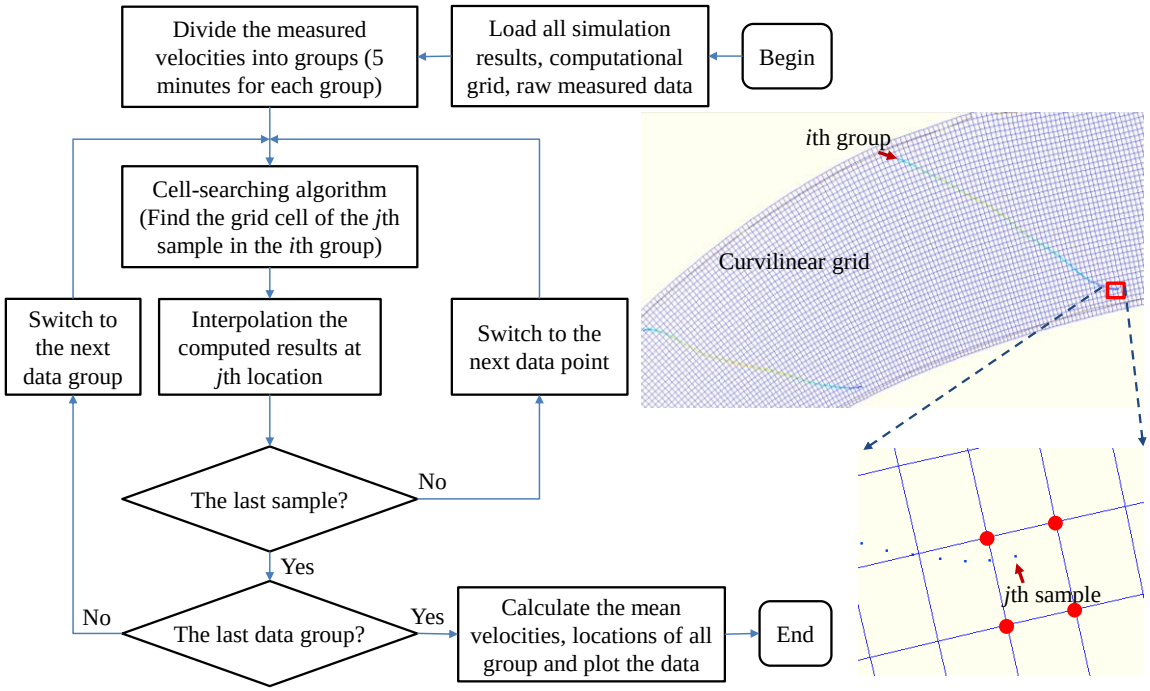

Figure 5-4. The algorithm to estimate the model result of the spatio-temporally depth-averaged velocity.

5.3 Results and discussions

5.3.1 The problems of the flow model in Chapter 4

Figure 5-5 shows the measured values and estimated results of water level at Station A, depth-averaged velocity over the upstream cross-section, and spatio-temporally depth-averaged velocity of the flow model in Chapter 4. The results show that the estimated values are reasonable agreement with measured values; however, the gaps between them have remained. Figure 5-5(a) indicates that the estimated tidal range is significantly smaller than measurements. The possible reasons are the influence of the strange tidal data from 1985 to 1990 as presented in Figure 5-2. Figure 5-5(b) demonstrates that the flow model reproduced well the mean velocities at the upstream location, but the predicted values are smaller than the field data, especially in the low tide. The spatio-temporally depth-averaged velocity also reveals the same trend and display the notable gaps between measurements and computations that also occurred clearly in the low tide in the near estuary and upstream areas. These gaps may be results of eliminating the upstream freshwater discharge and downstream tributary effect of Channel 2. Furthermore, the gap becomes larger after the location of Channel 2 as depicted in Figure 5-5 (c).

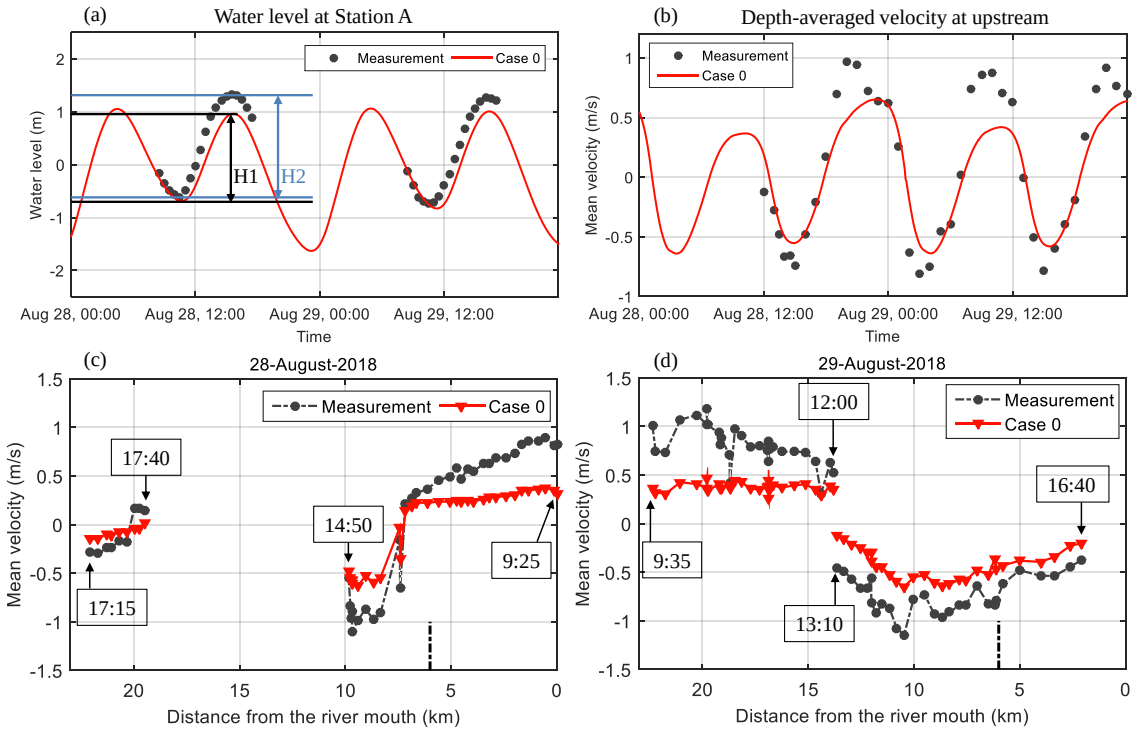

Figure 5-5. The measurement data and simulation results of Chapter 4's model: Water level at Station A (a), the depth-averaged velocity at upstream, and spatio-temporally depth-averaged velocity on 28th, 29th August 2018.

In this chapter, the flow model of My Thanh River was improved by concentrating on solving these above problems. Tidal data of the nearby station from 2008 to 2014 were used to predict the tide at the estuary of My Thanh River in 2018, abnormal tidal data from 1985 to 1990 were removed to decide the new constituents for configuring the downstream boundary Tide-BC. The upstream freshwater discharge was estimated by compensating the upstream mean discharge based on the simulation and measurement values. The simplified flow model of Channel 2 was also conducted to reduce the gap of spatio-temporally depth-averaged velocity near the estuary.

5.3.2 Review of tidal data

After reviewing the tidal data, estimated water levels at Station A and Station B have increased their ranges and were more agreement with the measured values as displayed in Figure 5-6. The optimization occurred on both amplitude and phase lag of the estimated tide. In terms of amplitude, the new tide has increased its high-water elevation, while

nearly remaining its low-water elevation. This explains why the model depth-averaged velocity over the upstream location has mainly risen in high tide.

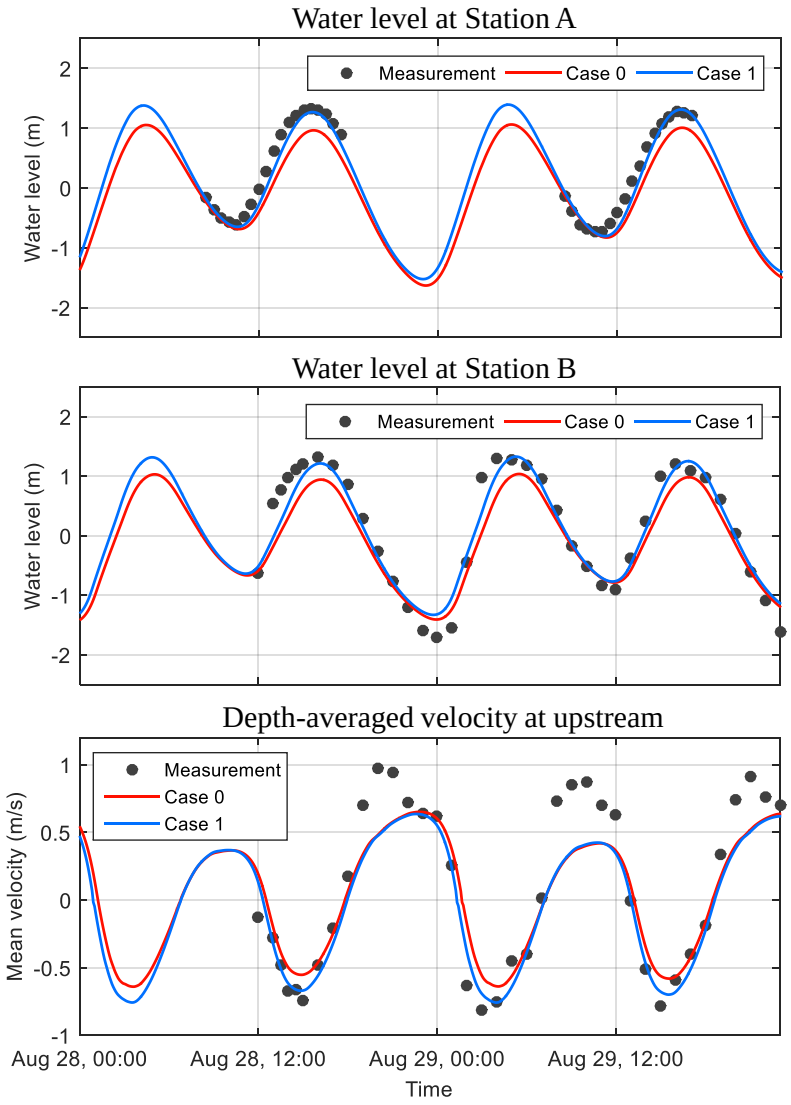

Figure 5-6. Measurement and estimated water level at Station A, Station B, and depth-averaged velocity at the upstream of Case 0 and Case 1, the negative velocity means that the water flows to the upstream-ward direction.

The errors of the estimated spatio-temporally depth-averaged velocity were calculated by the following equation:

$$e_i = \bar{v}_i - v_i \tag{19}$$

where, $\bar{v}_i$ and v_i denote the estimated and measured values of the spatio-temporally depth-averaged velocity, respectively. The results depicted in Figure 5-7 show that modifying the tide has affected the flow field in the whole river, especially in high tide because the new estimated tide has mainly increased in the high-water level as shown in Figure 5-6. The errors indicate that new tide has reduced significantly the errors in high tide and slightly decreased in low tide.

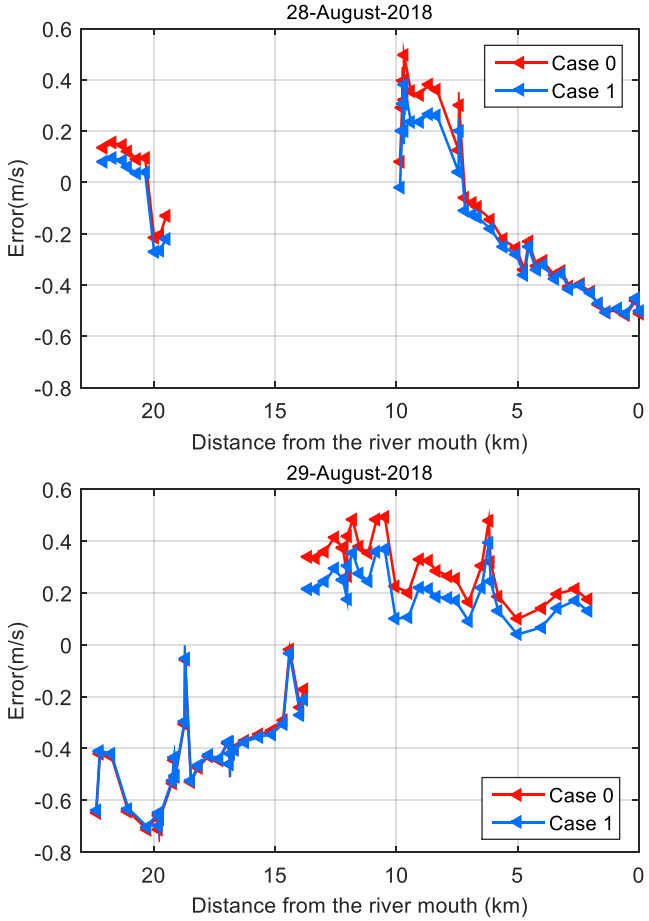

Figure 5-7. Errors of the estimated spatio-temporally depth-averaged velocity on 28th and 29th August 2018 of simulation Case 0 and Case 1.

5.3.3 Consideration of upstream discharge

The upstream discharge has not been considered in Chapter 4 making the imbalance of water discharge at the upstream boundary as mentioned in Sect. 5.2.3.1. Figure 5-8 shows the cumulative discharge of the flow model in Case 1, Case 2, and Case 3 after four

simulation days, the negative value represents for the discharge to upstream direction larger than the discharge to the downstream direction. This figure demonstrates that after four simulation days the mean discharge at Riemann-BC1 of Case 1 ($\bar{Q}_1$) equals -158 m^3/s or an imbalance has occurred. As mention above, to balance the water discharge at Riemann-BC1, $-\bar{Q}_1$ was used as the setting values of Discharge-BC1 and Discharge-BC2 boundaries. After that, the values of these open boundaries were compensated until $\bar{Q}_1$ approaches to zero value. The simulation result shows that with a total discharge of 220 m^3/s added to Discharge-BC1 and Discharge-BC2 boundaries (Case 2) would make $\bar{Q}_1$ = 0 m^3/s or the water discharge at the Riemann-BC1 was balanced.

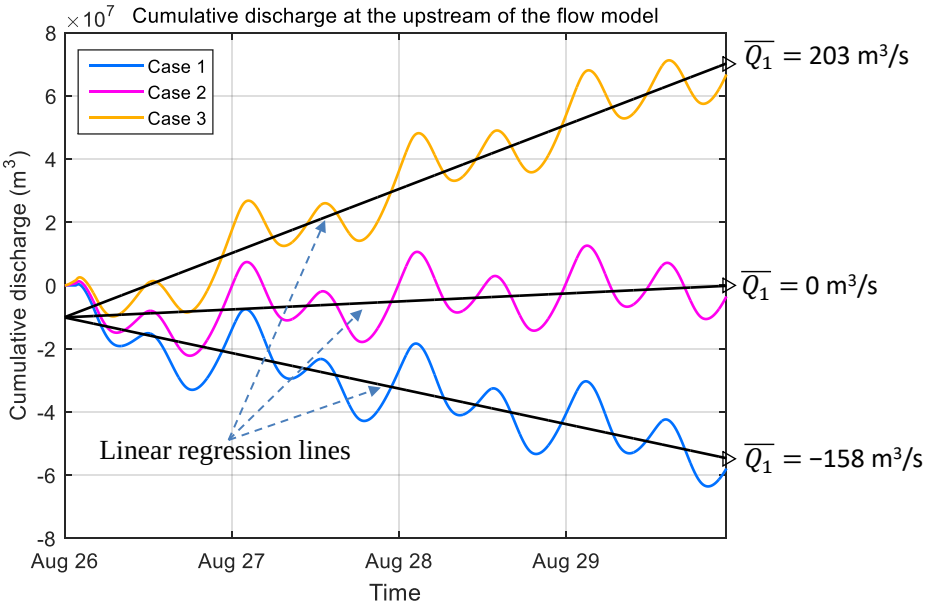

Figure 5-8. Cumulative discharges at Riemann-BC1 of simulation Case 1, Case 2, and Case 3.

However, the rivers in the VMD are under the effect of the upstream freshwater discharge originated from other rivers and human activities as agriculture, aquaculture, and industry. The measured discharge in August 2018 shows that mean discharge at the upstream cross-section in 36 hours equals 203 m^3/s (i.e. downstream-ward discharge is larger upstream-ward discharge). It means that an imbalance of the discharge occurs at the upstream, so the total value of Discharge-BC1 and Discharge-BC2 boundaries must be increased to accelerate the downstream-ward instantaneous discharge. The solution is adding 203 m^3/s

to the current values of Discharge-BC1 and Discharge-BC2, and these values were compensated again until the new value of $\bar{Q}_1$ approximated field value. Figure 5-8 shows that with a total discharge of 500 m^3/s (Case 3) the new value of $\bar{Q}_1$ has been equalled 203 m^3/s and the mean discharge at the upstream cross-section is 200 m^3/s very close to the field value. The increase of the upstream discharge mainly affects the estimated depth-averaged velocity at the upstream and spatio-temporally depth-averaged velocity as shown in Figure 5-9 and Figure 5-10, respectively. These graphs indicate that additional discharge at upstream boundaries was inversely influenced on the water velocity, it speeds up the downstream-ward velocity, while slowing down the upstream-ward velocity.

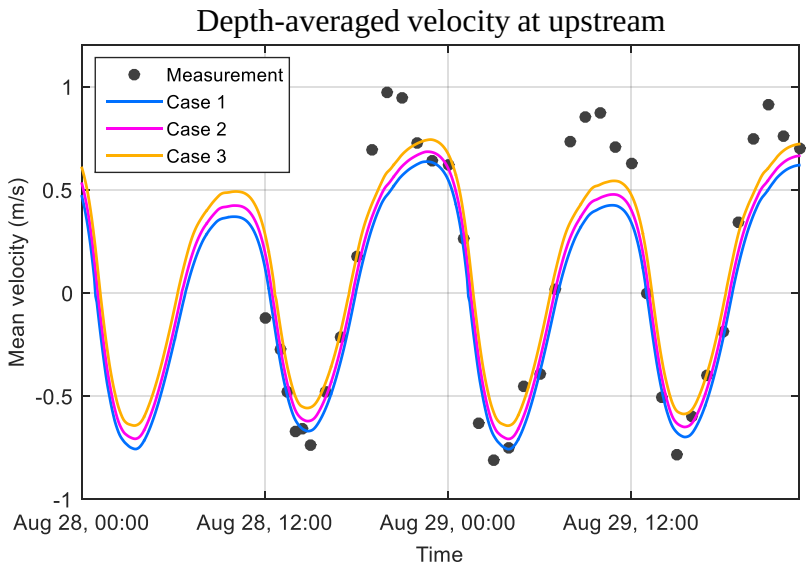

Figure 5-9. Measurement and estimated depth-averaged velocity at the upstream of Case 1, Case 2, and Case 3.

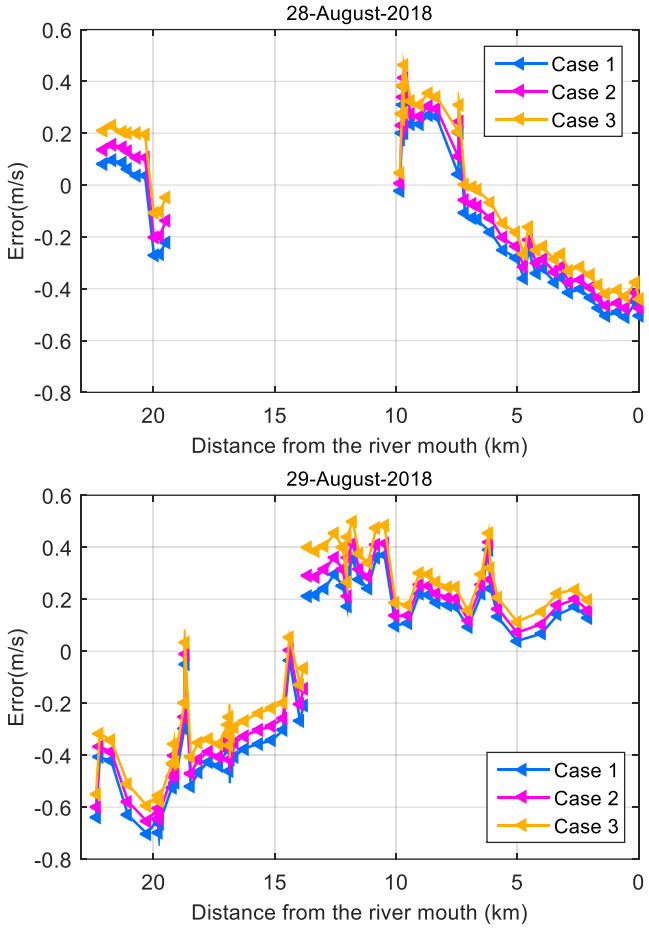

Figure 5-10. Errors of the estimated spatio-temporally depth-averaged velocity on 28th and 29th August 2018 of simulation Case 1, Case 2, and Case 3.

5.3.4 Consideration of the downstream tributary effect

Riemann Boundary was also applied to configure the upstream open boundary of the simplified model of the Channel 2 (Riemann-BC2). The value of this boundary was calibrated by balancing the water discharge technique as applying for Riemann-BC1. However, Channel 2 is lack of all related data, so the Riemann-BC2 value was calibrated by using its mean value as described in the Sect. 5.2.3.2.

Figure 5-11 shows that the average discharge of Riemann-BC2 in Case 4 ($\overline{Q}_2$) after four simulation days is 71 m^3/s. It means that the upstream-ward discharge is larger than the downstream-ward discharge because the Channel 2 direction is perpendicular to the main

river. The mean velocity at Riemann-BC2 ($\bar{u}_2$) could be calculated by using $\overline{Q}_2$ and the area of cross-section A_2 as the following:

$$\bar{u}_2 = \frac{\bar{Q}_2}{A_2} = \frac{71}{742} = 0.10, \quad (20)$$

and the mean value of the estimated water level at Riemann-BC2 ($\bar{\zeta}_2$) equals 0.09 m. By using $-\bar{u}_2$ and $\bar{\zeta}_2$, the new mean value of Riemann-BC2 calculated by equation (17) equals -0.20 m/s. This value of $\bar{F}_{R2}$ was used as a new value of Riemann-BC2 and compensated by simulating the model in Case 5 until $\overline{Q}_2$ closes to zero value. The final value of $\bar{F}_{R2}$ is -0.23 m/s which could make $\overline{Q}_2$ equal -5 m^3/s or the downstream-ward discharge slightly larger than the upstream-ward discharge.

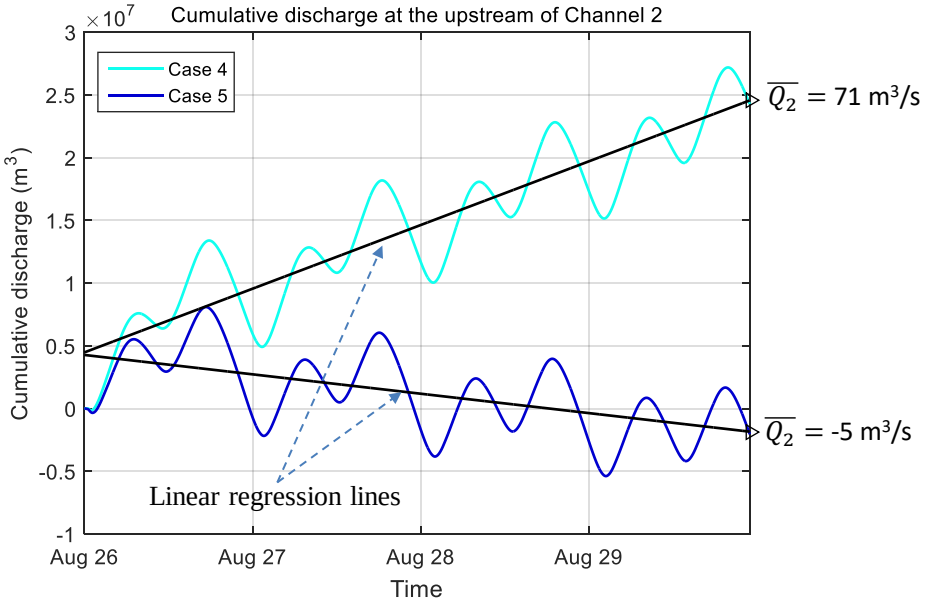

Figure 5-11. Cumulative discharges at Riemann B.C.2 of simulation Case 4 and Case 5.

Figure 5-12 and Figure 5-13 illustrate the effect of Channel 2 on the results of the flow model. The water levels at Station A and Station B were slightly decreased in the low tide and nearly remained values in the high tide as shown in Figure 5-12. This is the reason for the decrease of depth-averaged velocity at the upstream. However, the errors of estimated spatio-temporally depth-averaged velocity revealed that the simplified model of Channel 2 has significantly influenced the spatial velocity of My Thanh River from

around its mouth to the estuary in both high and low tide. This simplified model has also affected the upstream spatial velocity of My Thanh River, but the effect is minor as shown in Figure 5-12.

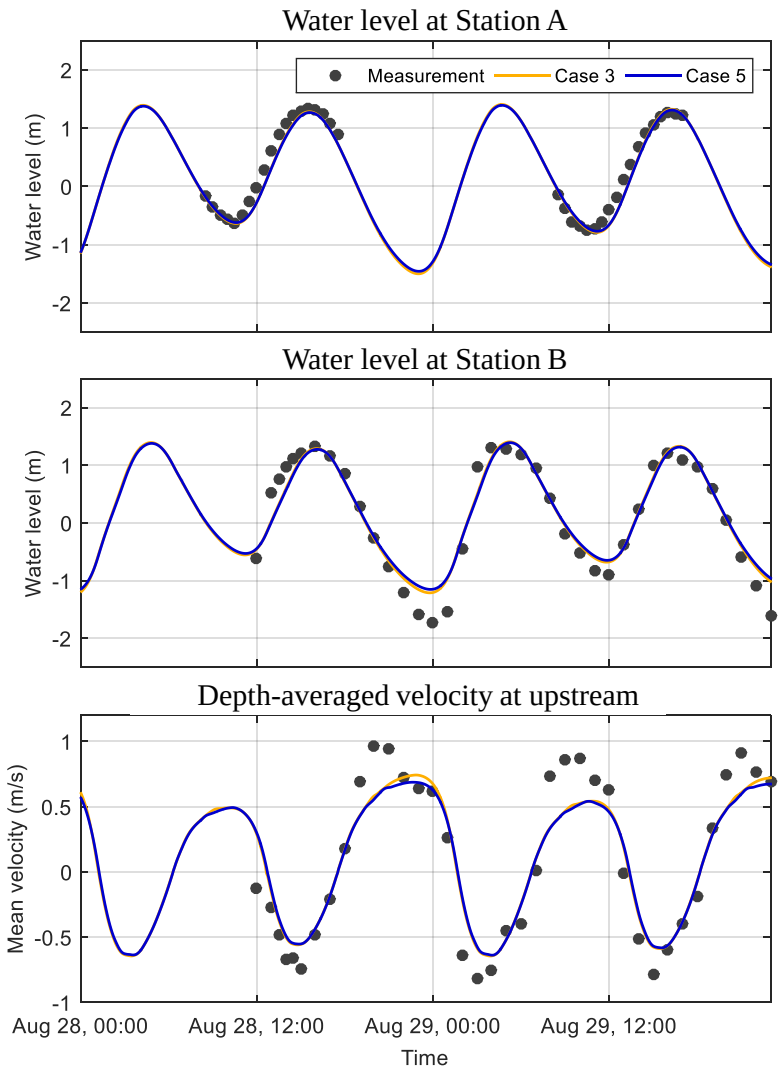

Figure 5-12. Measurements and estimated water level at Station A, Station B, and depth-averaged velocity at the upstream of Case 3 and Case 5.

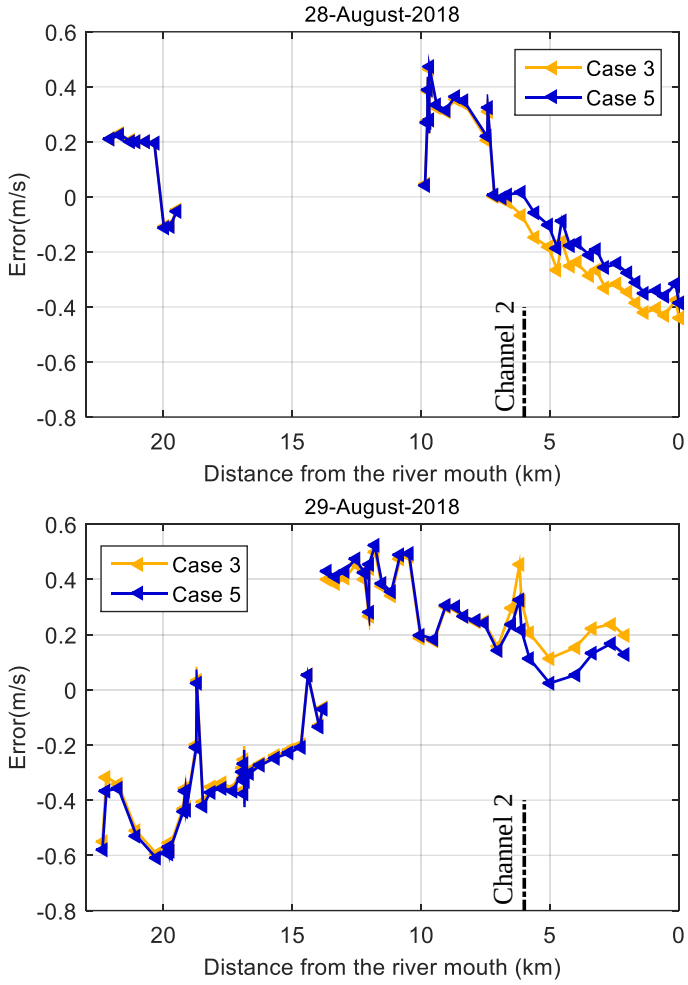

Figure 5-13. Errors of the estimated spatio-temporally depth-averaged velocity on 28th and 29th August 2018 of simulation Case 3 and Case 5.

5.3.5 Model comparison

After considering all potential factors, the 2-D flow model of My Thanh River in Chapter 4 (Case 0) was improved significantly. The new model (Case 5) has optimized both water level and velocity at fixed locations and the spatio-temporal velocity as shown in Figure 5-14 and Figure 5-15, respectively. After removing the strange data from 1985 to 1990, the downstream boundary could reproduce better water levels. It is demonstrated in the good agreement between the measured and estimated water level at the Station A location where close the downstream boundary.

The estimated water level at Station B in Case 5 was also better than Case 0, but the graphs still display large gaps in the low tide that might be caused by two possible reasons. The first is the national datum (VN-2000) is unavailable at Station B, the water level is only referred on the mean value of the measured level in the measurement period. The real water level might be shifted up or down. The second is the large difference between the simulation and the real bottom roughness of My Thanh River. The model was simulated with the linear change of the bottom roughness from downstream to upstream of the flow model, while the real bottom roughness might be more complicated because of the natural vegetation as mangroves in both banks of My Thanh River.

The depth-averaged velocity at the upstream location was also improved in both low tide and flood tide. The improvement mainly occurred after reviewing tidal data and considering the upstream discharge. Adding the simplified model of Channel 2 to the flow model has a minor effect on the velocity at the upstream.

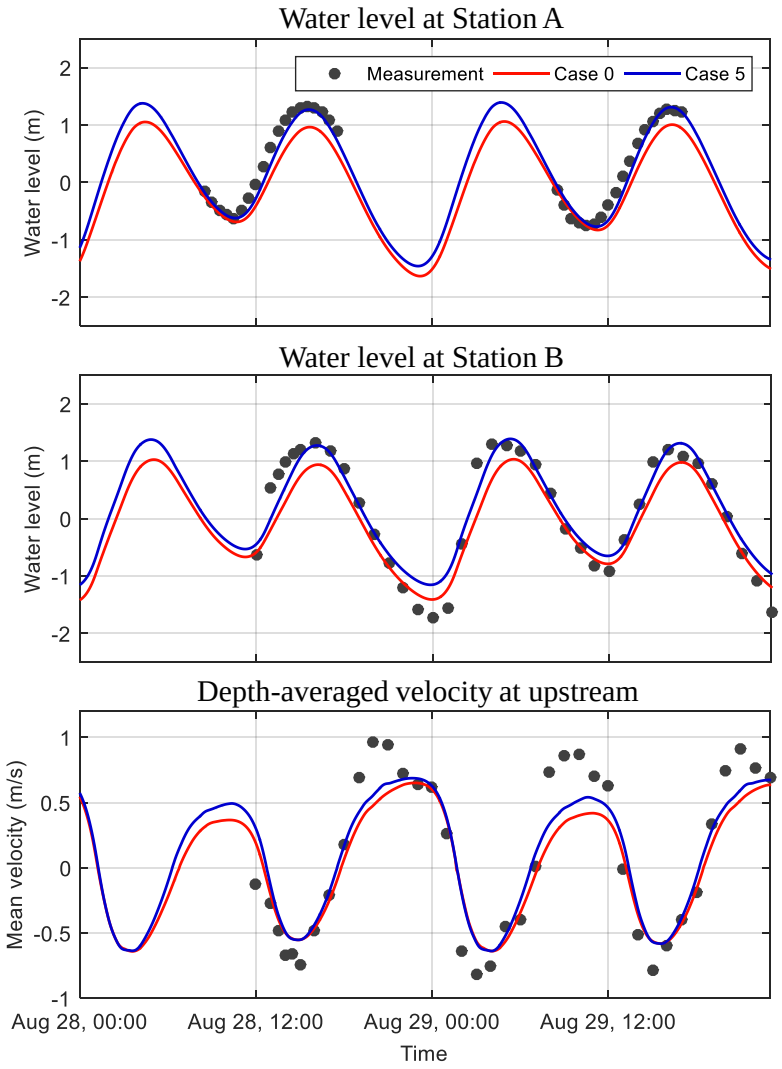

Figure 5-14. Measurement and estimated water level at Station A, Station B, and depth-averaged velocity at the upstream of Case 0 and Case 5.

The new model of My Thanh River shows the enhancement of the estimated spatio-temporally depth-averaged velocity along the river, especially after adding the simplified model of Channel 2. The errors of the estimated spatio-temporally depth-averaged velocity decreased in both stages of the tide, except the estimated velocity near the upstream location on 28th August 2018 and in the middle of the river on 29th August 2018 as shown in Figure 5-15. The increase of errors may be caused by the difference in the phase of spatial velocity because these velocities were collected around the time when the water flow was changing its direction (slack water). The notable improvement of errors was found after adding the model of Channel 2. It indicates that the tributary effects

play an important role in the flow model of the tidal rivers and should be involved in the modeling process.

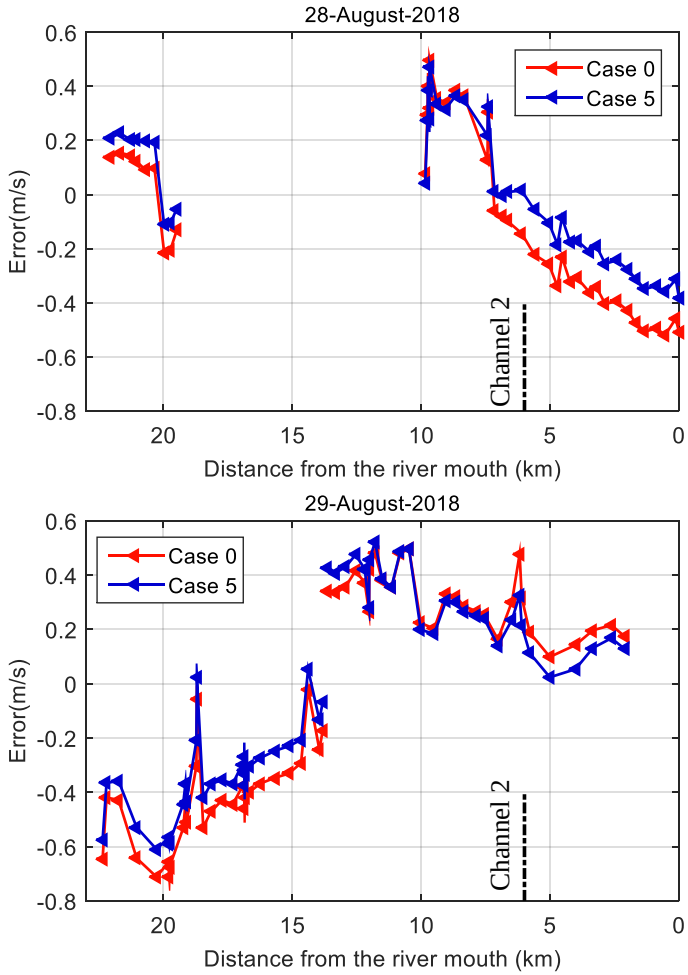

Figure 5-15. Errors of the estimated spatio-temporally depth-averaged velocity on 28th and 29th August 2018 of simulation Case 0 and Case 5.

To evaluate how the new 2-D flow model of My Thanh River was improved, the RMSE of the results were calculated by using the following equation:

$$\mathrm{RMSE} = \sqrt{\frac{1}{\mathrm{N}}\sum_{i=1}^{N}(\hat{m}_i - m_i)^2} \qquad (21)$$

where N is the number of field data points, $\hat{m}_i$ and m_i are computation and measurement values, respectively. Table 5-4 illustrates the RMSE values of the 2-D flow model for six simulation cases. The table shows that the water level at the Station A location was

improved sharply after removing the abnormal tidal data, the RMSE value decreased by 50% from 0.32 m to 0.16 m, and nearly remained value after considering the upstream discharge and the tributary effect. The water level at the Station B location is affected significantly by upstream discharge and tributary effect, the new flow model only improved 9% the estimated water level at this location, in terms of RMSE value. For the depth-averaged velocity at the upstream cross-section, the improvement was found mainly after considering the upstream discharge, the tributary effect slightly influenced the velocity at this cross-section. The RMSE value of this velocity was declined by 12%. Finally, the estimated spatio-temporally depth-averaged velocity was also improved notably, the RMSE value was decreased by 16%. The spatio-temporal velocity indicated a crucial role in investigating the influence of small channels to the main river which can not be realized by using velocity at the upstream cross-section.

Table 5-4. RMSE values the 2-D flow model.

RMSEs	Water level at Station A (m)	Water level at Station B (m)	Depth-average velocity at upstream (m/s)	Spatio-temporally depth-averaged (m/s)
Case 0	0.32	0.32	0.25	0.37
Case 1	0.16	0.26	0.24	0.34
Case 2	0.16	0.26	0.21	0.33
Case 3	0.15	0.27	0.21	0.32
Case 4	0.16	0.29	0.22	0.31
Case 5	0.16	0.29	0.22	0.31

5.3.6 Flow model validation with June 2018 data

The calibrated model was simulated in the first measurement period (16th – 17th June 2018) to validate its performance. The collected dataset is the same with the measurement in August 2018, including water level at Station A during the bathymetric data measurement, depth-averaged velocities over the upstream cross-section in 36-hours with

some missing points because of the heavy rain, and depth-averaged velocity along the river in two days by using ADCP.

The results in Figure 5-16 and Figure 5-17 present that the calibrated model could run stably in the first measurement period, all water levels and velocities described well the tendencies of the measured data. However, some discrepancies have remained between measured and computed results. This might be caused by the changing of the flow conditions of My Thanh River in the middle of June 2018 compared with them at the end of August 2018. Rivers in the VMD are strongly affected by the seasonal fluctuation, and June is the month at the early of the flood season, the flow conditions must be very different after about 2.5 months later when in the middle of the flood season. However, the validation results show that the method in this study can be applied to approximately investigate the flow field of a river with the least measured data.

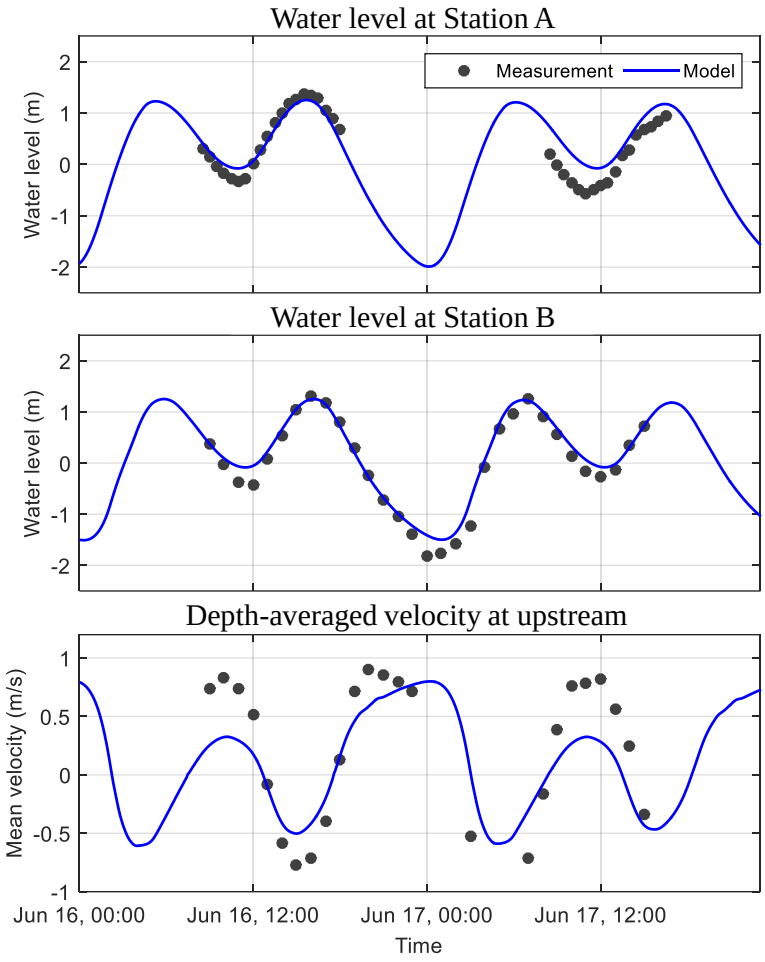

Figure 5-16. Measurement and estimated water level at Station A, Station B, and depth-averaged velocity at the upstream on 16th, 17th June 2018.

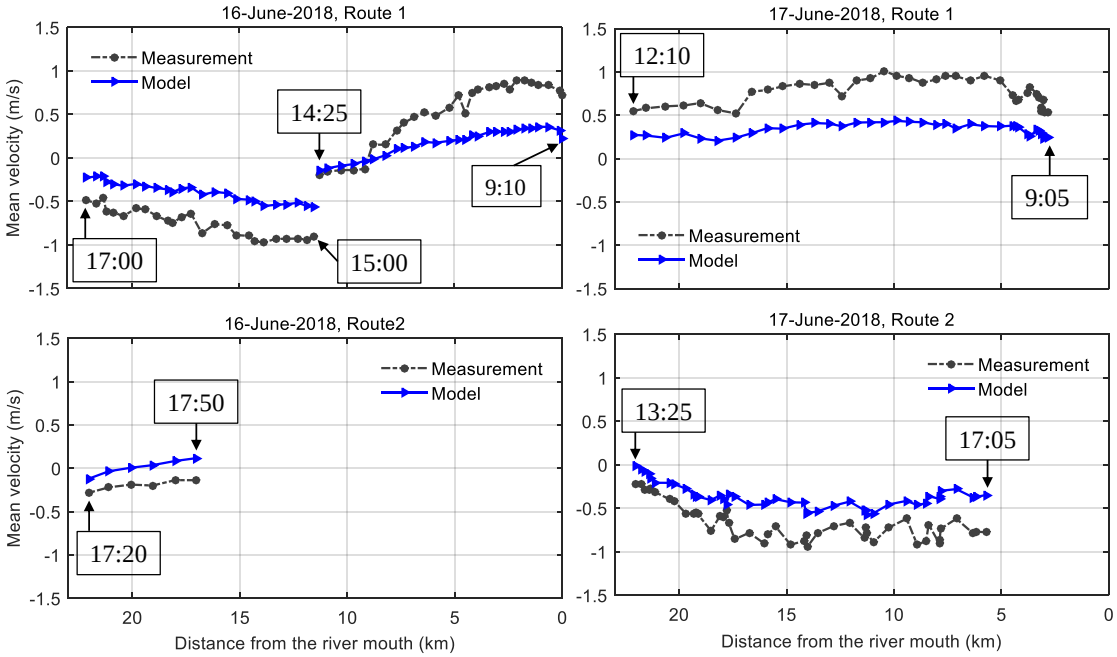

Figure 5-17. Errors of the estimated spatio-temporally depth-averaged velocity on 16th and 17th June 2018.

5.3.7 Discussions and future works

The results in this chapter present that a new model has successfully optimized the flow field of My Thanh River after reviewing the tidal data, taking into account the upstream freshwater discharge, and conducting the simplified flow model of a small channel near the estuary. The measured spatio-temporal velocity along My Thanh River indicated a crucial role in the calibrating process. By comparing the computation and measurement of them, it demonstrated that the small channels can improve the flow field of small tidal rivers which could not be found out by using measured data at fixed locations. While most of the recent studies have been calibrating the model only based on the data at some specific locations, using spatio-temporal data is a new calibrating method that can optimize the quality of the flow model of the rivers. In this study, after considering all potential factors, the new flow model has already declined the RMSE values of predicted water levels near the estuary and upstream of the study river 50% and 9%, respectively; the depth-averaged velocity at upstream and the spatio-temporally depth-averaged velocity of the study river 12% and 16%, respectively, in terms of RMSE values. Further,

due to working with spatio-temporal data, an algorithm was also developed to calculate the computation values of the spatio-temporal velocity over the computational domain. This algorithm can be applied with various kinds of data from a 2-D model, such as river depth, water level, salinity, suspended sediment concentrations, water quality, and so on. The proposed algorithm can be upgraded for calibrating the parameters of the 3-D model based on spatial measured data.

The simplified 2-D model of the small channel (Channel 2) implemented in the situation of totally inadequate data has also improved the velocities near the estuary. This channel was modeled by a straight canal that has been applied by Moftakhari *et al.* (2016) and Theol *et al.* (2019) to conduct the numerical experiments for their real canals and had reasonable results. In the VMD, the coastal rivers have many small channels on both sides, and most of them have sluice gates near their mouth to prevent the saltwater enters the in-land paddy fields. They are manually opened some times in a year to drain out the waste-water back to the rivers. According to the local people, this waste-water has negative effects on the river ecosystem, especially shrimps and fishes. Hence, finding out suitable ways to control such gates to reduce their influences might be very necessary to study. Because these canals completely lack data, our modeling method for small channel combining with the Real-time control feature of Delft3D (Deltares, 2017) will be a good option for modeling them and create the operating scenarios for numerical experiments of the sluice gates.

Although the new model already optimized the flow field, the discrepancies between estimated and measured values are still large. It may be caused by some other factors which were eliminated from the model. First, there are no depth samples at near-bank areas, our assumption might be not correct because the real bedforms of these areas are very complicated. Hence, the velocities near riverbank zones may be actually underestimated. Second, My Thanh is a tidal river, its salinity changes due to seasonality, and large difference between mouth and upstream. In fact, in June 2018, the measured value of salinity is ~28.5 ppt and ~3 ppt at the river mouth and upstream cross-section, respectively; whereas, in August 2018, the salinity decreased to ~7.5 ppt and ~1 ppt at the river mouth and upstream, respectively. However, the salinity transport was not simulated, this may be a reason for the discrepancy because if saltwater is not mixed well

with the freshwater, the mechanism of the flow will be very complicated. Last but not least, no discharge data in the upstream boundary was proved to cause the large differences in velocity because there is no driving force to control the flow velocity (Takagi *et al.*, 2019). Therefore, finding new ways to control the river velocities and involving salinity transport into the current model is necessary for future works.

5.4 Conclusions of the improvement of 2-D flow model of small tidal river

This chapter mainly concentrated on the optimization of the 2-D flow model of My Thanh River in Chapter 4. The method in this chapter enabled using the spatio-temporal velocity collected by the ADCP device to calibrate the parameters of the 2-D flow model besides the field data at the fixed locations. The simulation results indicate that the estimated flow field of the new model has been improved after reviewing tidal data at My Thanh station and the nearby station, considering the influence of the upstream freshwater discharge, and downstream tributary effect of the small channel (Channel 2). Especially, the effect of the small channels could be detected only by the spatio-temporally depth-averaged velocity because of the mild influence on the upstream flows. This finding shows the promising application of spatio-temporal velocity and the small channels in conducting the flow model of the rivers. The new model could also run stably in the other periods when the flow conditions of the river have small changes. Finally, the method in this study can be applied on other rivers with similar conditions to investigate their flow fields serving for other studies in the future as sediment transport and morphological changes, riverbank erosion and retreat, salinity intrusion, storm surge or flooding and risk which are mainly based on the flow model of the rivers.

Chapter 6 Conclusions

The flow field of the rivers plays a crucial role in investigating the other fluvial processes as sediment transport and morphological changes, riverbank erosion and retreat, salinity intrusion, storm surge, or flooding and risk. In the VMD, all rivers are under the effects of the tidal regime of the East Sea and the Gulf of Thailand, and most of the small rivers are lack of hydrodynamic and hydrographic data, except the tidal data. As a result, applying and calibrating the 2-D flow model for these rivers are a big challenge. The objective of this study is to demonstrate how to apply and calibrate the 2-D flow model for small tidal rivers in the VMD with insufficient hydrographic data. First, a new searching method for finding the depth samples for the recent interpolators (IDW, RBF, and OK) is proposed to improve the estimated river bathymetry, especially near riverbank regions. Second, the simplified 2-D flow model suggested by Takagi *et al.* (2019) was applied with some adjustments to the small tidal rivers with only tidal data available at the estuary. Finally, the applied 2-D flow model was optimized by reviewing the historical tidal data and re-calibrating the parameters based on measured data at fixed locations and along the river. The followings are the main conclusions of the present study.

Searching methods were realized that play an important role in riverbed interpolation, especially in the case of applying on sparse depth dataset. The recent searching methods as elliptical search and rectilinear search indicated their drawback when putting in sparse zigzag depth samples. The recent interpolators applying these searching methods underestimated the depth of the near riverbank areas where the width of the river highly changes. However, the proposed searching method, named curvilinear search, could solve this drawback and the estimated bathymetry is smoother and more exact than elliptical and rectilinear search. The comparison results show that the curvilinear search operating with IDW interpolator and the regional interpolators are suitable methods that can work effectively with sparse depth data like the zigzag dataset. However, more studies should be conducted in the future to further refining the estimated bathymetry, such as find out good planning for the zigzag measurement strategy, improving near-bank region measurement, and supporting more grid types.

The simplified 2-D flow model suggested by Takagi *et al.* (2019) could be applied to My Thanh River, a small tidal river in the VMD, using the estimated bathymetry from the proposed interpolation methods with insufficient hydraulic data. This model only requires the tidal data for configuring the downstream open boundary, and at upstream the Riemann Boundary was applied instead of the discharge boundary. Riemann Boundary is the key point of applying the 2-D flow model to a small tidal river with insufficient hydrodynamic data. However, the built-in Riemann Boundary in Delft 3D was found that is the main reason for the underestimated flow field around the boundary. By suggesting the extended Riemann Boundary, the estimated flow field has been improved and the proposed 2-D flow model will be very helpful for other river-related studies in the future such as sediment transport, riverbed morphology development, riverbank erosions, riverbank failures.

The 2-D flow model in this study was improved significantly after reviewing the tidal data and considering the upstream freshwater discharge. By analyzing the yearly changes of the primary constituents at My Thanh station from 1985 to 2007 and Tran De station (about 10km from My Thanh station) from 2008 to 2014, the tidal data from 1985 to 1990 was removed because of the unnatural variation trends of the primary constituents. Besides, the imbalance of the water discharge of the model caused by using the Riemann Boundary with zero value was also found out and solved by compensating the upstream discharge with the mean value of the simulation discharge. A mean value of measured discharge was also put on the upstream to represent the mean value of freshwater discharge. The simulation results of the flow model with the new tide indicate that the model has optimized significantly, especially the estimated water level near the downstream which was improved 50% in terms of RMSE value. The flow model has successfully involved the effect of the upstream freshwater discharge; however, the simulation average discharge is smaller than the measurement value. It demonstrates that the 2-D flow model in this study is only suitable with the tidal rivers which are under small effect from the upstream freshwater.

A simplified method to build the 2-D flow model of a small channel (Channel 2) near the downstream of the My Thanh River which is lack of data was also proposed to consider the tributary effects to the flow model of the main river. The open boundary of the

Channel 2 model (Riemann-BC2) was also utilized the Riemann Boundary, its value was calibrated based on two general steps. First, the flow model was simulated with a zero value of Riemann-BC2 to calculate the mean value of Riemann-BC2 ($\bar{F}_{R2}$) using the mean velocity and mean water level at this boundary. Second, The opposite sign value of $\bar{F}_{R2}$ can be used as the new value of Riemann-BC2 to balance the discharge at upstream of the small channel. The results of the 2-D model of My Thanh river with Channel 2's model show that adding the model of the small channel was mainly improved the spatio-temporally depth-averaged from around its mouth to the estuary. After considering all factors, the velocity at the upstream location and the spatio-temporally depth-averaged velocity were improved 12% and 16%, respectively, in terms of RMSE values.

The proposed 2-D flow model of My Thanh River was demonstrated that it could be run stably in other periods when the flow conditions have minor changes. The proposed model was simulated to investigate the flow field of My Thanh River in the middle of June 2018 (about 2.5 months before the calibrating periods) to validate the model. The results proved that the model could operate stably, but the notable discrepancies were found. The possible reason is the differences of flow conditions between two periods, June is the beginning of flood season while August is the middle of flood season in the VMD.

In summary, the 2-D flow model successfully applied to the small tidal river with insufficient hydrodynamic and hydrographic data in the present study. The proposed flow model can be potentially applied for studying the flow field of the new small tidal rivers quickly with the least measurement works. This flow information is very helpful for analyzing storm surge, flooding and risk, or in coupling with other models like the sediment transport model, morphological model, salinity transport model to investigate riverbank erosion and retreat, salinity intrusion of the small tidal rivers in the VMD.

Acknowledgment

This study is funded in part by the Can Tho University Improvement Project VN14-P6, supported by a Japanese ODA loan.

I would like to thank my supervisor Prof. Akio OKAYASU and my co-supervisors Prof. Tsuyoshi IKEYA and Assoc. Prof. Daisuke INAZU for the patience, enthusiastic supervision, guidance, inspiration, and encouragement to pursue this Ph.D. I also would like to thank Prof. Kazuo TANI (Tokyo University of Marine Science and Technology), Assoc. Prof. Van Pham Dang TRI (Program E2, ODA project, Can Tho University), Assoc. Prof. Nguyen Chi NGON and Dr. Tran Thanh HUNG (College of Engineering and Technology, Can Tho University) for valuable advice and contributions. It is such a privilege to work with extraordinary scholars like you.

I would like to thank Dr. Van Pham Dang THUY, Ms. Chau Thi Phuong UYEN, Ms. Ayana TANAKA, Ms. Kanae KUITA for kindly supporting me in financial issues and daily living activities, without you I believe that I can not survive and have a very smooth life in Japan. Special thanks also go to Rie TEJIMA sensei for giving me very interesting Japanese lessons.

I would like to acknowledge the support and guidance of the field survey team of program E2, ODA project, and many other students for their support during the fieldwork. Thanks go to Mr. Nguyen Thanh QUAN who has assisted in all field activities in Vietnam during my doctoral course.

My appreciation also goes to the colleagues at the Department of Automation and Technology, College of Engineering Technology, Can Tho University for the valuable support my works during my study period in Japan. The constructive comments of anonymous reviewers and editors from journals where several contents of this Ph.D. were published are greatly appreciated.

Finally, I would like to thank my lovely wife Tran Ngoc DANG for her support, encouragement, and patience. To my son and my daughter for surviving many days without their father close by. To my dear parents for the amazing support to my family while I was away, my brothers, sister, and for my entire family and friends in Can Tho and Ben Tre provinces.

References

(DHI) Danish Hydraulic Institute 2017a. MIKE 11: A Modelling System for Rivers and Channels, Reference Manual.

(DHI) Danish Hydraulic Institute 2017b. MIKE 21 Flow Model: Hydrodynamic Module, User Guide.

(USACE) U. S. Army Corps of Engineers 2016a. HEC-RAS: River Analysis System. Hydraulic Reference Manual, 2D Modeling User's Manual, Version 5.0, February, Hydrologic Engineering Center, California.

(USACE), U. S. Army Corps of Engineers 2016b. HEC-RAS: River Analysis System. Hydraulic Reference Manual, Version 5.0, February, Hydrologic Engineering Center, California.

Andes, L. C. and Cox, A. L. 2017. Rectilinear Inverse Distance Weighting Methodology for Bathymetric Cross-Section Interpolation along the Mississippi River. *Journal of Hydrologic Engineering*, 22(7).

Bi, Q. and Toorman, E. A. 2015. Mixed-sediment transport modelling in Scheldt estuary with a physics-based bottom friction law. *Ocean Dynamics*, 65(4), 555-587.

Bovee, K. D. 1996. Perspectives on two-dimensional river habitat models: the PHABSIM experience. *Proceedings of Second International Symposium on Habitat Hydraulics Ecohydraulics 2000,* Volume B, 149-162.

Burroughes, J., George, K. and Abbott, V. 2001. Interpolation of hydrographic survey data. *The Hydrographic Journal*, (99), 21-23.

Carter, G. S. and Shankar, U. 1997. Creating rectangular bathymetry grids for environmental numerical modelling of gravel-bed rivers. *Applied Mathematical Modelling*, 21(11), 699-708.

Caviedes-Voullième, D., Morales-Hernandez, M., Lopez-Marijuan, I. and García-Navarro, P. 2014. Reconstruction of 2D river beds by appropriate interpolation of 1D

cross-sectional information for flood simulation. *Environmental Modelling & Software,* 61, 206-228.

Chen, S., Cowan, C. F. N. and Grant, P. M. 1991. Orthogonal Least Squares Learning Algorithm for Radial Basis Function Networks. *IEEE Transactions on Neural Networks,* 2(2), 302-309.

Chen, W.-B. and Liu, W.-C. 2017. Modeling the Influence of River Cross-Section Data on a River Stage Using a Two-Dimensional/Three-Dimensional Hydrodynamic Model. *Water,* 9(3).

Chen, W., Chen, K., Kuang, C., Zhu, D. Z., He, L., Mao, X., Liang, H. and Song, H. 2016. Influence of sea level rise on saline water intrusion in the Yangtze River Estuary, China. *Applied Ocean Research,* 54, 12-25.

Chirokov, A., 2006. *Scattered Data Interpolation and Approximation using Radial Base Functions* [online]. MATLAB Central File Exchange. Available from: https://www.mathworks.com/matlabcentral/fileexchange/10056-scattered-data-interpolation-and-approximation-using-radial-base-functions [Accessed 6 March 2020].

Conner, J. T. and Tonina, D. 2014. Effect of cross-section interpolated bathymetry on 2D hydrodynamic model results in a large river. *Earth Surface Processes and Landforms,* 39(4), 463-475.

Deltares, 2014a. *Delft3D-FLOW manual* [online]. Available from: https://oss.deltares.nl/documents/183920/185723/Delft3D-FLOW_User_Manual.pdf [Accessed 6 March 2020].

Deltares, 2014b. *Delft3D-QUICKPLOT User Manual* [online]. Available from: https://oss.deltares.nl/documents/183920/185723/Delft3D-QUICKPLOT_User_Manual.pdf [Accessed 6 March 2020].

Deltares 2017. Delft3D-Flow, Simulation of multi-dimensional hydrodynamic flows and transport phenomena, including sediments, User Manual, Version 3.15.52614, October 2017, 686 pp.

Deltares, 2020a. *Delft3D-TIDE User Manual* [online]. Available from: https://content.oss.deltares.nl/delft3d/manuals/Delft3D-TIDE_User_Manual.pdf [Accessed 12 July 2020].

Deltares, 2020b. *RGFGRID User Manual* [online]. Available from: https://content.oss.deltares.nl/delft3d/manuals/RGFGRID_User_Manual.pdf [Accessed 6 March 2020].

Deng, S., Xia, J., Zhou, M. and Lin, F. 2019. Coupled modeling of bed deformation and bank erosion in the Jingjiang Reach of the middle Yangtze River. *Journal of Hydrology,* 568, 221-233.

Diaconu, D. C., Bretcan, P., Peptenatu, D., Tanislav, D. and Mailat, E. 2019. The importance of the number of points, transect location and interpolation techniques in the analysis of bathymetric measurements. *Journal of Hydrology,* 570, 774-785.

Elias, E. P. L., Gelfenbaum, G. and Van der Westhuysen, A. J. 2012. Validation of a coupled wave-flow model in a high-energy setting: The mouth of the Columbia River. *Journal of Geophysical Research: Oceans,* 117(C9), n/a-n/a.

Falcão, A. P., Matias, M. P., Pestana, R. and Gonçalves, A. B. 2016. Methodology to Combine Topography and Bathymetry Data Sets for Hydrodynamic Simulations: Case of Tagus River. *Journal of Surveying Engineering,* 142(4).

Fissel, D., Birch, R. and Jiang, J., 2002. Three-dimensional computational flow modeling and high resolution flow surveys for fisheries environmental studies on the upper Columbia River. ed. *Proceedings of Hydro Vision 2002 conference*, 2002 Portland, Oregon.

Goff, J. A. and Nordfjord, S. 2004. Interpolation of Fluvial Morphology Using Channel-Oriented Coordinate Transformation: A Case Study from the New Jersey Shelf. *Mathematical Geology,* 36, 643–658.

Hai, P. T., Masumoto, T. and Shimizu, K. 2006. Evaluation of Flood Regulation Role of Paddies in The Lower Mekong River Basin using a 2D Flood Simulation Model. *Annual Journal of Hydraulic Engineering, JSCE,* 50, 73-78.

Hilldale, R. C. and Raff, D. 2008. Assessing the ability of airborne LiDAR to map river bathymetry. *Earth Surface Processes and Landforms,* 33(5), 773-783.

Hilton, J. E., Grimaldi, S., Cohen, R. C. Z., Garg, N., Li, Y., Marvanek, S., Pauwels, V. R. N. and Walker, J. P. 2019. River reconstruction using a conformal mapping method. *Environmental Modelling & Software,* 119, 197-213.

Hong, B. and Shen, J. 2012. Responses of estuarine salinity and transport processes to potential future sea-level rise in the Chesapeake Bay. *Estuarine, Coastal and Shelf Science,* 104-105, 33-45.

Ijaz, M. W., Mahar, R. B., Ansari, K. and Siyal, A. A. 2019. Optimization of salinity intrusion control through freshwater and tidal inlet modifications for the Indus River Estuary. *Estuarine, Coastal and Shelf Science,* 224, 51-61.

Islam, M., Hofstra, N. and Sokolova, E. 2018. Modelling the Present and Future Water Level and Discharge of the Tidal Betna River. *Geosciences,* 8(8).

Jeong, S., Yeon, K., Hur, Y. and Oh, K. 2010. Salinity intrusion characteristics analysis using EFDC model in the downstream of Geum River. *Journal of Environmental Sciences,* 22(6), 934-939.

Kasvi, E., Salmela, J., Lotsari, E. and Lane, S. N. 2019. Comparison of remote sensing based approaches for mapping bathymetry of shallow, clear water rivers. *Geomorphology,* 333, 180-197.

Kondolf, G. M., Schmitt, R. J. P., Carling, P., Darby, S., Arias, M., Bizzi, S., Castelletti, A., Cochrane, T. A., Gibson, S., Kummu, M., Oeurng, C., Rubin, Z. and Wild, T. 2018. Changing sediment budget of the Mekong: Cumulative threats and management strategies for a large river basin. *Sci Total Environ,* 625, 114-134.

Krüger, R., Karrasch, P. and Bernard, L., 2018. Evaluating Spatial Data Acquisition and Interpolation Strategies for River Bathymetries. *Geospatial Technologies for All.* 3-25.

Kuang, C., Zhao, F., Song, H., Gu, J. and Dong, Z. 2020. Morphological responses of a long-narrow estuary to a restoration scheme and a major storm. *Marine Geology,* 427.

Lai, Y. G., Thomas, R. E., Ozeren, Y., Simon, A., Greimann B. P. and Wu, K. 2015. Modeling of multilayer cohesive bank erosion with a coupled bank stability and mobile-bed model. *Geomorphology*, 243, 116-129.

Li, J. and Heap, A. D. 2008. A Review of Spatial Interpolation Methods for Environmental Scientists. *Geoscience Australia*, Record 2008/23, 137pp.

Lin, G.-F. and Chen, L.-H. 2004. A spatial interpolation method based on radial basis function networks incorporating a semivariogram model. *Journal of Hydrology*, 288(3-4), 288-298.

Lin, Y.-T., Chen, W. B., Su, Y. F., Han, J. Y. and Jang, J. H. 2018. Improving river stage forecast by bed reconstruction in sinuous bends. *Journal of Hydroinformatics*, 20(4), 960-974.

Merwade, V. 2009. Effect of spatial trends on interpolation of river bathymetry. *Journal of Hydrology*, 371(1), 169-181.

Merwade, V. M., Maidment, D. R. and Goff, J. A. 2006. Anisotropic considerations while interpolating river channel bathymetry. *Journal of Hydrology*, 331(3-4), 731-741.

Moftakhari, H. R., Jay, D. A. and Talke, S. A. 2016. Estimating river discharge using multiple‐tide gauges distributed along a channel. *Journal of Geophysical Research: Oceans*, 121(4), 2078-2097.

Pebesma, E. J. 2004. Multivariable geostatistics in S: the gstat package. *Computers & Geosciences*, 30(7), 683-691.

Pham Van, C., Brye, B. D., Deleersnijder, E., Hoitink, A. J. F., Sassi, M., Spinewine, B., Hidayat, H. and Soares-Frazão S. 2016. Simulations of the flow in the Mahakam river–lake–delta system, Indonesia. *Environmental Fluid Mechanics*, 16(3), 603-633.

Rahdarian, A. and Niksokhan, M. H. 2017. Numerical modeling of storm surge attenuation by mangroves in protected area of mangroves of Qheshm Island. *Ocean Engineering*, 145, 304-315.

Ramm, J., 2011. *Kriging and Inverse Distance Interpolation using GSTAT* [online]. MATLAB Central File Exchange. Available from: https://www.mathworks.com/matlabcentral/fileexchange/31055-kriging-and-inverse-distance-interpolation-using-gstat [Accessed 6 March 2020].

Rinaldi, M., Mengoni, B., Luppi, L., Darby, S. E. and Mosselman, E. 2008. Numerical simulation of hydrodynamics and bank erosion in a river bend. *Water Resources Research,* 44(9).

Rousseau, Y. Y., Van de Wiel, M. J. and Biron, P. M. 2017. Simulating bank erosion over an extended natural sinuous river reach using a universal slope stability algorithm coupled with a morphodynamic model. *Geomorphology,* 295, 690-704.

Sciortino, J. A., 2010. *Fishing harbour planning, construction and management.* Rome, Italy: FAO.

Shintani, C. and Fonstad, M. A. 2017. Comparing remote-sensing techniques collecting bathymetric data from a gravel-bed river. *International Journal of Remote Sensing,* 38(8-10), 2883-2902.

Takagi, H., Quan, N. H., Anh, L. T., Thao, N. D., Tri, V. P. D. and Anh, T. T. 2019. Practical modelling of tidal propagation under fluvial interaction in the Mekong Delta. *International Journal of River Basin Management,* 17(3), 377-387.

Takagi, H., Thao, N. and Anh, L. 2016a. Sea-Level Rise and Land Subsidence: Impacts on Flood Projections for the Mekong Delta's Largest City. *Sustainability,* 8(9).

Takagi, H., Tsurudome, C., Thao, N. D., Anh, L. T., Ty, T. V. and Tri, V. P. D. 2016b. Ocean tide modelling for urban flood risk assessment in the Mekong Delta. *Hydrological Research Letters,* 10(1), 21-26.

Thanh, V. Q., Reyns, J., Wackerman, C., Eidam, E. F. and Roelvink, D. 2017. Modelling suspended sediment dynamics on the subaqueous delta of the Mekong River. *Continental Shelf Research,* 147, 213-230.

Theol, S. A., Jagers, B., Suryadi, F. X. and Fraiture, C. D. 2019. The Role of Gate Operation in Reducing Problems with Cohesive and Non-Cohesive Sediments in Irrigation Canals. *Water,* 11(12).

Thi Ha, D., Ouillon, S. and Van Vinh, G. 2018. Water and Suspended Sediment Budgets in the Lower Mekong from High-Frequency Measurements (2009–2016). *Water,* 10(7).

Tran Anh, D., Hoang, L. P., Bui, M. D. and Rutschmann, P. 2018. Simulating Future Flows and Salinity Intrusion Using Combined One- and Two-Dimensional Hydrodynamic Modelling—The Case of Hau River, Vietnamese Mekong Delta. *Water,* 10(7).

Tri, V. P. D., Trung, N. H. and Thanh, V. Q. 2013. Vulnerability to Flood in the Vietnamese Mekong Delta: Mapping and Uncertainty Assessment. *Journal of Environmental Science and Engineering B2,* 229-237.

Trung, L. V., 2018. *Riverbank erosion under boat-generated wave attacks and proposed countermeasures for wave attenuation.* (PhD). Saitama Universuty, Saitama, Japan.

Tuoitrenews, 2018. *Vietnamese ministry introduces land subsidence map in Mekong Delta* [online]. Available from: https://tuoitrenews.vn/news/society/20180619/vietnameseministry-introduces-land-subsidence-map-in-mekongdelta/46227.html [Accessed June 13 2020].

van der Wegen, M., Jaffe, B. E. and Roelvink, J. A. 2011. Process-based, morphodynamic hindcast of decadal deposition patterns in San Pablo Bay, California, 1856-1887. *Journal of Geophysical Research: Earth Surface,* 116(F2).

Van, P. D. T., Popescu, I., van Griensven, A., Solomatine, D. P., Trung, N. H. and Green, A. 2012. A study of the climate change impacts on fluvial flood propagation in the Vietnamese Mekong Delta. *Hydrology and Earth System Sciences,* 16(12), 4637-4649.

Xie, Q., Yang, J., Lundstrom, S. and Dai, W. 2018. Understanding Morphodynamic Changes of a Tidal River Confluence through Field Measurements and Numerical Modeling. *Water,* 10(10).

Xie, Q., Yang, J. and Lundström, T. 2019. Field Studies and 3D Modelling of Morphodynamics in a Meandering River Reach Dominated by Tides and Suspended Load. *Fluids,* 4(1).

Yin, Y., Karunarathna, H. and Reeve, D. E. 2019. Numerical modelling of hydrodynamic and morphodynamic response of a meso-tidal estuary inlet to the impacts of global climate variabilities. *Marine Geology,* 407, 229-247.

Zarzuelo, C., Lopez-Ruiz, A. and Ortega-Sanchez, M. 2019. Evaluating the impact of dredging strategies at tidal inlets: Performance assessment. *Sci Total Environ,* 658, 1069-1084.

Zhang, R., He, J., Zhao, Y., Peng, Y. and Fu, L. 2013. Another Important Factor of Rising Sea Level: Soil Erosion. *CLEAN - Soil, Air, Water,* 41(2), 174-178.